Pergamon   **PII: S0038–092X(01)00054–8**

www.elsevier.com/locate/solener

PARAMETERIZED TRANSMITTANCE MODEL FOR DIRECT BEAM AND CIRCUMSOLAR SPECTRAL IRRADIANCE

CHRISTIAN A. GUEYMARD[†]

174 Bluebird Lane, Bailey, CO 80421, USA

Abstract—An upgraded spectral radiation model called SMARTS2 (Simple Model of the Atmospheric Radiative Transfer of Sunshine) is introduced. The solar shortwave direct beam irradiance is calculated from spectral transmittance functions for the main extinction processes in the cloudless atmosphere: Rayleigh scattering, aerosol extinction, and absorption by ozone, uniformly mixed gases, water vapor, and nitrogen dioxide. Temperature-dependent or pressure-dependent extinction coefficients have been developed for all these absorbing gases, based on recent spectroscopic data obtained either directly from the experimental literature or, in a preprocessed form, from MODTRAN, a state-of-the-art rigorous code. The NO_2 extinction effect, in both the UV and visible, is introduced in detail for the first time in a simple spectral model by taking into account temperature-dependent absorption coefficients. Aerosol extinction is evaluated using a two-tier Ångström approach. Parameterizations of the wavelength exponents and single-scattering coefficient for different aerosol models (proposed by Shettle and Fenn, Braslau and Dave, and also in the Standard Radiation Atmosphere) are provided as a function of both wavelength and relative humidity. Moreover, aerosol turbidity can now be estimated from airport visibility data using a function based on the Shettle and Fenn aerosol model. SMARTS2 also has an optional circumsolar correction function and two filter smoothing functions which together allow the simulation of actual spectroradiometers. This facilitates comparison between modeled results and measured data. Preliminary performance assessment indicates that the direct-beam irradiance predicted by the proposed model compares well to published reference spectra obtained with rigorous radiative codes, and to measured spectroradiometric data. © 2001 Elsevier Science Ltd. All rights reserved.

1. INTRODUCTION

Spectral solar irradiance models are needed in a variety of applications spread among different disciplines such as atmospheric science, biology, health physics and energy technology (photovoltaic systems, high performance glazings, daylighting, selective coatings, etc.). In particular, Nann and Bakenfelder (1993) describe 12 possible uses of spectral radiation models for solar energy systems and buildings applications. Two general types of spectral irradiance models may be used to predict or analyze solar radiation at the Earth's surface: sophisticated rigorous codes and simple transmittance parameterizations. A well known example of the first kind is the LOWTRAN family, which originated more than 20 years ago. It has been supplanted by an even more detailed code called MODTRAN (Anderson *et al.*, 1993; Berk *et al.*, 1989). This type of model considers that the atmosphere is constituted of different layers, and thus uses reference or measured

vertical profiles of the gaseous and aerosol constituents.

Because of the required detailed inputs, execution time, and some output limitations, rigorous codes such as MODTRAN are not appropriate for all applications, particularly those in engineering. Most of the latter needs are presently filled by parameterized models which are relatively simple compared to MODTRAN. A number of these simple models have appeared in the literature since the early 1980s (Bird, 1984; Bird and Riordan, 1986; Brine and Iqbal, 1983; Gueymard, 1993a; Justus and Paris, 1985; Matthews *et al.*, 1987; Nann and Riordan, 1991). These models are based on Leckner's (1978) landmark contribution. For computerized engineering calculations, the Fortran code SPCTRAL2 (Riordan, 1990), based on Bird (1984) and Bird and Riordan (1986), has been frequently used. A preliminary version of the present model, SMARTS1 (Gueymard, 1993a), consisted of some improvements over SPCTRAL2, but still used Leckner's core functions. The new version of the model presented here is fundamentally new. A detailed reexamination of his approach appears justified

[†]ISES member. E-mail: cgueymard@mac.com

because much fundamental knowledge on gaseous absorption and aerosols has been added since his work. Furthermore, data of higher spectral resolution are now available, improving the detail in those spectral regions where gaseous absorption changes rapidly with wavelength.

This contribution develops the derivation of the part of SMARTS2 concerned with direct beam irradiance. The remaining parts of the model predicting diffuse and global irradiance incident on horizontal or inclined surfaces will be detailed separately. There are six main objectives and achievements in this study.

- Increase the spectral resolution of the transmittance calculations.
- Introduce more accurate transmittance functions for all the atmospheric extinction processes, with consideration for temperature and humidity effects.
- Add nitrogen dioxide (NO_2) to the list of absorbers, with temperature-dependent absorption coefficients.
- Include highly accurate absorption coefficients from recent spectroscopic data.
- Add the capability to estimate the circumsolar enhancement factor for realistic comparison with radiometric data.
- Add the flexibility to smooth the output irradiances using simulated radiometric filters.

The direct-beam transmittance is evaluated here at 1881 wavelengths from the lower end of UV-B (280 nm) to the practical high-end of the short-wave spectrum, 4000 nm. A constant interval of 1 nm is considered between 280 and 1700 nm, and of 5 nm between 1705 and 4000 nm, with a transitional wavelength at 1702 nm. This is to be compared, for instance, to a total of 127 wavelengths for Leckner's model, or 122 wavelengths at widely varied intervals for Bird and Riordan's model or SPCTRAL2.

The present resolution may be considered low by spectroscopists, just right by atmospheric physicists, or rather high by engineers. The 1-nm constant interval within the most important part of the spectrum is considered here as a good compromise between resolution and model complexity. The model's outputs (spectral transmittances and irradiances) can easily be downgraded afterwards if so desired by the user (see Section 6).

2. REFERENCE ATMOSPHERES

Ten different reference atmospheres are proposed. They consist of different vertical profiles of temperature, pressure, and of the concentrations of the main gases of the atmosphere. The main features of six of these reference atmospheres are described by Anderson *et al.* (1986) and are also used in the LOWTRAN and MODTRAN families: US Standard Atmosphere (USSA), Mid Latitude Summer (MLS), Mid Latitude Winter, Sub Arctic Summer, Sub Arctic Winter, and Tropical. Four supplementary atmospheres have been constructed for this work from other basic reference profiles (Anon., 1966): Sub Tropical Summer, Sub Tropical Winter, Arctic Summer, and Arctic Winter. All profiles are defined with a vertical increment of generally 1 km. Below the highest altitude considered here for reference calculations (4 km), a four-point Lagrange interpolation scheme is used to smooth the vertical profile of each quantity listed above. Because ozone (O_3) and NO_2 are normally largely concentrated in the stratosphere, their total abundance does not vary appreciably whenever the site altitude is below 4 km. For greater accuracy, a factor, $C_t = 1 - 0.00898z$, can correct their total abundance at sea-level from the altitude, z, in km, using a linear fit based on the reference atmospheres' data.

A nominal or 'effective' ozone temperature, T_{eo}, is defined as the weighted average of the concentration and temperature discretized profiles of the reference atmospheres (Anderson *et al.*, 1986; Anon., 1966). This results in an average of 213 to 235.7 K for a sea-level site depending on the reference atmosphere.

Relative humidity has been calculated from the mixing ratio of water vapor tabulated by Anderson *et al.* (1986), using the method described by Kneizys *et al.* (1980). (Relative humidity is an important 'interactive parameter' that influences the size and optical properties of atmospheric aerosols, as will be shown in Section 3.6; it may also be used to estimate precipitable water, as mentioned in Section 3.5.)

Individual total column abundances are calculated in different ways. The total reduced thickness (in atm-cm) of O_3 and NO_2 is available for the six reference atmospheres considered in LOWTRAN or MODTRAN. For the four supplementary atmospheres, new representative ozone values had to be proposed. The reference latitudes associated with these atmospheres helped provide the needed ozone values, using average seasonal ozone distributions for the period 1957–1975 (London, 1977) and the composite satellite data tabulated by Keating *et al.* (1990). Typical total NO_2 columns for the four supplementary atmospheres are selected from the limited data reviewed in Section 3.3.

For water vapor, the incremental precipitable water, Δw, for an incremental atmospheric column of height Δz (normally 1 km) has been calculated from $\Delta w = \rho_v \, \Delta z$, where the water vapor density, ρ_v, is determined from the discretized humidity profile tabulated by Anderson *et al.* (1986) using the perfect gas laws. The total precipitable water above each level, w, is then obtained by Simpson's rule of integration.

For oxygen (O_2) and carbon dioxide (CO_2), two of the most important absorbing gases in the shortwave spectrum, an effective reduced height, or scaled height, for a real (i.e. inhomogeneous) path has been obtained by scaling the actual density profiles with a Curtis–Godson approximation, in a way similar to Pierluissi and Tomiyama (1980) and Leckner (1978):

$$u_g = \int_z^\infty \left(\frac{p(h)}{p_0}\right)^n \left(\frac{T_1}{T(h)}\right)^m \left(\frac{\rho_a(h)}{\rho_{a0}}\right) dh \qquad (1)$$

where $p(h)$, $T(h)$ and $\rho_a(h)$ are, respectively, the pressure, temperature and air density at level h, $p_0 = 1013.25$ mb, $T_1 = 288.15$ K, $\rho_{a0} = 1.225$ kg/m^3, and n and m are variable coefficients calculated for different gases and conditions by Pierluissi and Tsai (1987). They are taken here for O_2 and CO_2 as $n = 0.9353$ and 0.79, and $m = 0.1936$ and -1.3244, respectively.

Specific atmospheric conditions can be used instead of one of the reference atmospheres. If the site is not at sea level, it is necessary to correct the effective temperatures of O_3 and NO_2 for the difference between the sea-level and ground-level temperatures. This can be done roughly by extrapolating the selected atmospheric temperature profile as though the site were on a virtual tower having its base at sea-level. In so doing, the possibility of at least one inversion layer must be taken into account. Such inversions frequently occur below 0°C as revealed by radiosonde soundings (Gueymard, 1994).

The numerical solution of Eq. (1), obtained for the 10 reference atmospheres described above, has been fitted to the O_2 and CO_2 scaled heights as a function of the site-level pressure, p, and temperature, T:

$$u_g = c_0 \, P^{c_1} \theta^{c_2} \qquad (2)$$

where $P = p/p_0$, and $\theta = T_1/T$. The coefficients take the following values: for O_2, $c_0 = 4.9293$ km, $c_1 = 1.8849$, $c_2 = 0.1815$, and for CO_2, $c_0 = 4.8649$ km, $c_1 = 1.9908$, and $c_2 = -0.697$.

If the site pressure is not known, it can be estimated from the site altitude and latitude according to the curve fit provided by Gueymard (1993b).

3. DIRECT BEAM IRRADIANCE

Under cloudless sky conditions, direct beam radiation normally constitutes the major part of the incoming solar shortwave radiation, above about 400 nm. Moreover, its measurement can be used to derive information on atmospheric conditions or constituents (e.g. gaseous abundances and aerosol turbidity) by comparison with model calculations smoothed to approximate the instrument's spectral response. For these reasons, a major effort is devoted here to obtain accurate *individual* transmittance functions.

The beam irradiance received at ground level by a surface normal to the sun's rays at wavelength λ is given by

$$E_{bn\lambda} = E_{on\lambda} \, T_{R\lambda} \, T_{o\lambda} \, T_{n\lambda} T_{g\lambda} \, T_{w\lambda} T_{a\lambda} \qquad (3)$$

where $E_{on\lambda}$ is the extraterrestrial irradiance corrected for the actual sun–earth distance and the other factors are the transmittances for the different extinction processes considered here: Rayleigh scattering, absorption by ozone, nitrogen dioxide, uniformly mixed gases and water vapor, and finally, aerosol extinction.

3.1. Rayleigh scattering

The Rayleigh optical thickness was first evaluated directly from its theoretical expression (see, for example, Kerker (1969), and McCartney (1976)):

$$\tau_{R\lambda} = 24\pi^3 \frac{H_R}{N_0 \lambda^{-4}} \left(\frac{n_0^2 - 1}{n_0^2 + 2}\right)^2 \left(\frac{6 + 3\delta}{6 - 7\delta}\right) \qquad (4)$$

where H_R is the atmospheric scale height (8.4345 km at 15°C), N_0 is the number density of molecules (2.547305×10^{25} m^{-3} at 15°C), n_0 is the refractive index of air (an intricate function of wavelength), δ is the depolarization factor, and λ is the wavelength. This equation has been reevaluated using the most recent determinations of δ (0.0279, according to Young (1981)) and of n_0 (Peck and Reeder, 1972), as recommended by Teillet (1990). Calculations were repeated every 2 nm between 250 and 1000 nm, and every 5 nm beyond 1000 nm. A least-squares curve fit was then used to develop the following equation:

$$\tau_{R\lambda} = P/(a_1\lambda^4 + a_2\lambda^2 + a_3 + a_4\lambda^{-2}) \qquad (5)$$

where P is the pressure correction defined in Eq.

(2), $a_1 = 117.2594$ μm^{-4}, $a_2 = -1.3215$ μm^{-2}, $a_3 = 3.2073 \times 10^{-4}$, and $a_4 = -7.6842 \times 10^{-5}$ μm^2. Eq. (5) fits the 'exact' calculations obtained with Eq. (4) with a deviation <0.01% throughout the spectrum. This is an important improvement compared to a peak deviation of 3.4% at 540 nm (and larger deviations beyond 2000 nm) for the frequently used Leckner (1978) equation, and to an average deviation of about 1.5% for SMARTS1 and SPCTRAL2.

From Bouguer's law, the Rayleigh transmittance is then simply:

$$T_{R\lambda} = \exp(-m_R \tau_{R\lambda}), \qquad (6)$$

where m_R is the optical air mass, obtained from Eq. (A.1) in Appendix A.

3.2. Ozone absorption

The Bouguer law is also used to describe ozone absorption, i.e.

$$T_{o\lambda} = \exp(-m_o \tau_{o\lambda}) \qquad (7)$$

where

$$\tau_{o\lambda} = u_o A_{o\lambda} \qquad (8)$$

is the ozone optical thickness, m_o its optical mass (from Eq. (A.1)), u_o its reduced pathlength (in atm-cm), and $A_{o\lambda}$ its spectral absorption coefficient.

Ozone absorbs strongly in the UV, moderately in the visible, and slightly in the near infrared. Recent spectroscopic laboratory data from Daumont et al. (1992) are available for the Hartley–Huggins bands at 0.01 nm resolution. The original data (personal communication with Dominique Daumont) were smoothed in 1-nm steps, up to 344 nm. From 345 to 350 nm, data from Molina and Molina (1986) were downgraded from their original resolution of 0.5 nm. Between 351 and 355 nm, data from Cacciani et al. (1989) were used after smoothing to 1 nm. The same procedure was repeated between 356 and 365 nm, where the absorption coefficients were derived from the data in MODTRAN (based on unpublished data by Cacciani). The cut-off wavelengths of all these intervals were selected to reduce discontinuity at the blend between the different datasets.

A reference laboratory temperature, $T_{ro} = 228$ K, has been selected for all the datasets available to represent the basic absorption coefficients, $A_{o\lambda}(T_{ro})$. (These coefficients are not listed here for conciseness, but can be found in the SPEC-

TRM.DAT file, available online at ftp://alpha.f-sec.ucf.edu/public/smarts2 or http://homepage.mac.com/smarts2. This file also contains all the other necessary absorption coefficients, as well as the complete tabulation of the extraterrestrial spectral irradiance at all the 1881 wavelengths considered here.) Similar to Smith et al. (1992), a quadratic temperature correction is applied at other temperatures.

In the visible (Chappuis band) and near infrared (Wulf band), recent laboratory data (Anderson, 1992, 1993) were downgraded to 1-nm intervals. The temperature effect here being less important than in the Hartley–Huggins band, a linear temperature correction is sufficient between 407 and 560 nm, and is obtained by interpolation between the two datasets for 228 and 240 K. The original data showed significant temperature dependence up to 560 nm, and negligible dependence between 560 and 762 nm.

Finally, some very weak absorption bands are present above 3120 nm. The corresponding absorption coefficients were obtained by smoothing the MODTRAN transmittance results at 5-nm intervals up to 4000 nm and applying Eqs. (7) and (8) backwards.

The effect on the ozone transmittance of selecting two extreme nominal temperatures (210 and 240 K) is shown in Fig. 1 for a part of the Hartley–Huggins band. The jagged shape of these curves results from the detailed absorption structure characteristic of that band. At their peaks, these transmittances are significantly larger than
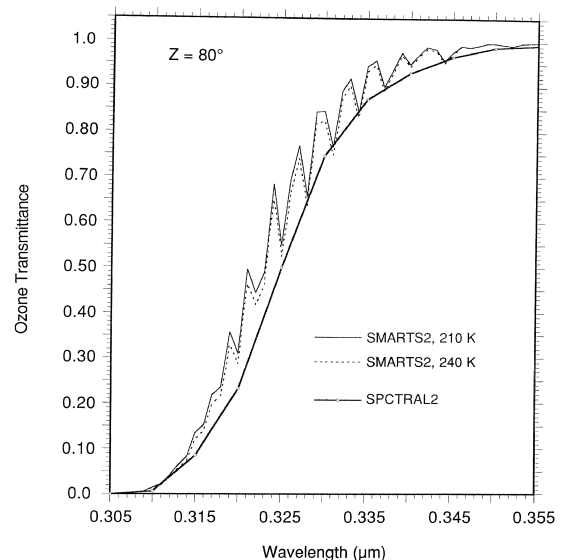

Fig. 1. Ozone transmittance predicted by SMARTS2 and SPCTRAL2 (Leckner's model) in the UV.

SPCTRAL2 or Leckner predictions, which use the same older absorption data from Vigroux (1953), no temperature correction, and a coarser step (5 nm in this band).

3.3. Nitrogen dioxide absorption

Like ozone, NO_2 transmittance is modeled with Bouguer's law, i.e.

$$T_{n\lambda} = \exp(-m_n u_n A_{n\lambda}) \qquad (9)$$

where m_n is the NO_2 optical mass from Eq. (A.1), u_n its reduced pathlength (in atm-cm), and $A_{n\lambda}$ its spectral absorption coefficient. NO_2 is a highly variable atmospheric constituent which plays a key role in the complex ozone cycle, both in the stratosphere, where it is naturally present, and in the troposphere, where its concentration may be high due to pollution. High concentrations of NO_2 over large cities are responsible in great part for the typical brown color of the pollution cloud (Husar and White, 1976). Total column measurements of NO_2 in an industrial city resulted in widespread values of u_n, ranging from 0.044 to 13 matm-cm, with a median of 1.66 matm-cm (Schroeder and Davies, 1987). For comparison, the six most-used reference atmospheres (Anderson *et al.*, 1986) list a total column of only about 0.2 matm-cm NO_2. Actual long-term measurements of the total NO_2 column for remote environments in both hemispheres show a typical seasonal pattern with a winter low of about 0.1 matm-cm and a summer high of about 0.2 matm-cm (Elansky *et al.*, 1984; McKenzie and Johnston, 1984). Only a limited number of references discuss the variability of the tropospheric and/or stratospheric NO_2 abundances (e.g. Coffey, 1988; Coffey *et al.*, 1981; Elansky, *et al.*, 1984; Kambezidis *et al.*, 2001; Liley *et al.*, 2000; McKenzie and Johnston, 1984; Mount *et al.*, 1984; Noxon, 1978, 1980; Song *et al.*, 1994), so that the NO_2 climatology is still insufficiently known — particularly in urban environments, where it is highly variable in both space and time.

The values of $A_{n\lambda}$ at different temperatures are derived from laboratory data (Davidson *et al.*, 1988) in the 280–624 nm range and smoothed to 1-nm intervals from their original resolution (0.514 nm). Between 625 and 700 nm, data from Schneider *et al.* (1987) are used. As with ozone, a dependence of the absorption coefficients on the nominal NO_2 temperature is considered here to extend the laboratory data. The reference temperature chosen here is $T_{rn} = 243.2$ K. For a nominal, or 'effective', temperature T_{en}, the absorption coefficients are obtained as:

$$A_{n\lambda}(T_{en}) = \text{Max}\left\{ 0, A_{n\lambda}(T_{rn}) \right.$$
$$\left. \times \left[1 + (T_{en} - T_{rn}) \sum_{i=0}^{i=5} f_i \lambda^i \right] \right\} \qquad (10)$$

where $f_0 = 0.69773$, $f_1 = -8.1829$, $f_2 = 37.821$, $f_3 = -86.136$, $f_4 = 96.615$, $f_5 = -42.635$, for $\lambda < 0.625$ μm, or else $f_0 = 0.03539$, $f_1 = -0.04985$, and $f_2 = f_3 = f_4 = f_5 = 0$.

The spectral transmittances for O_3 and NO_2 are compared in Fig. 2 for different total slant pathlengths, $m_o u_o$ and $m_n u_n$, respectively. These transmittances are almost equivalent in form but spectrally shifted when $m_n u_n$ is about a factor of 100 less than $m_o u_o$. This is equivalent to saying that NO_2 is about 100 times more efficient than ozone at absorbing radiation around their respective peak. However, it is also generally 20 to 10,000 times less abundant, so that its effect is significant, or more important than ozone, in polluted atmospheres only.

3.4. Uniformly mixed gas absorption

Some atmospheric constituents known as the 'mixed gases' (principally O_2 and CO_2) have both a monotonically decreasing atmospheric concentration with altitude and significant absorption bands in the infrared. Using the analysis of Pierluissi and Tsai (1986, 1987), the mixed gas transmittance is defined as:

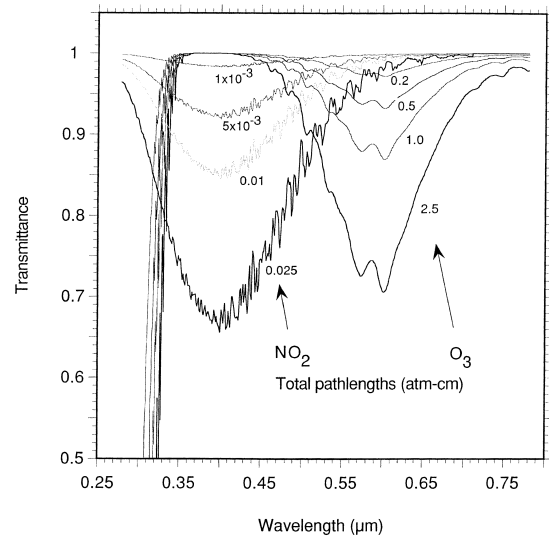$$T_{g\lambda} = \exp[-(m_g u_g A_{g\lambda})^a] \qquad (11)$$

Fig. 2. Ozone and nitrogen dioxide transmittances for different total pathlengths.

where $m_g = m_R$ is the gas optical mass from Eq. (A.1), $A_{g\lambda}$ is the spectral absorption coefficient, and u_g is the altitude-dependent gaseous scaled pathlength defined in Section 2. The value of u_g for O_2 is used below 1 μm and the value for CO_2 is used above, in accordance with their respective absorption spectra. The exponent a was obtained by averaging the data tabulated by Pierluissi and Tsai (1986, 1987): $a = 0.5641$ for $\lambda < 1$ μm, or else $a = 0.7070$. The values of $A_{g\lambda}$ were obtained by averaging MODTRAN transmittance results for different reference atmospheres, and inverting Eq. (11). The mixed gas transmittance as obtained from Eq. (11) for the Tropical reference atmosphere and a zenith angle of 80° is compared to other modeled values in Fig. 3. Compared to SMARTS2 or MODTRAN, prediction by Leckner's model (used in SPCTRAL2 and SMARTS1 for instance) is obviously very crude in this spectral band. Note also the extremely sharp transition between 759 and 760 nm, where the transmittance drops from 0.97 to 0.08 for the modeled atmospheric conditions, due to strong absorption by O_2.

3.5. Water vapor absorption

In the near infrared spectrum, water vapor is by far the most important absorber. The accurate determination of its transmittance is therefore of most importance here. To improve accuracy over previous models (e.g. Leckner's), the functional form proposed by Pierluissi et al. (1989) has been slightly modified as follows:

$$T_{w\lambda} = \exp\{ - [(m_w w)^{1.05} f_w^n B_w A_{w\lambda}]^c\} \qquad (12)$$
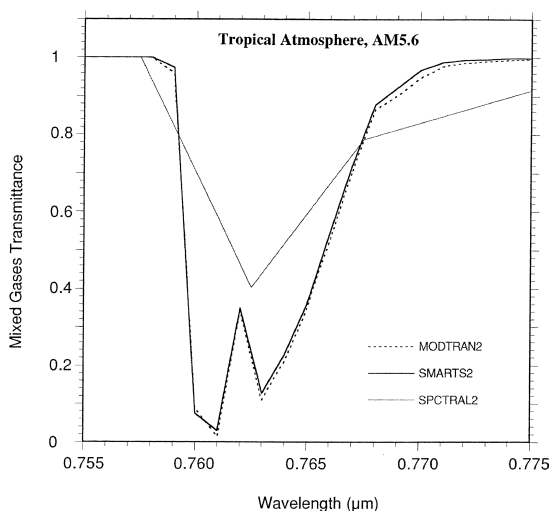

Fig. 3. Mixed gas transmittance in the visible for different models.

where m_w is the water vapor optical mass, w the total precipitable water, c and n are wavelength-dependent exponents, B_w is a correction factor taking into account that the absorption process varies with the distance from the band center, and f_w is a pressure scaling factor that compensates for inhomogeneities in the water vapor pathlength by application of the Curtis–Godson approximation (Koepke and Quenzel, 1978; Leckner, 1978; Pierluissi et al., 1989). The latter factor is obtained similarly to the mixed gases' reduced height, Eq. (1), except that no temperature correction is necessary for water vapor in the visible and near infrared (see, e.g. Asano and Uchiyama, 1987; Ridgway and Arking, 1986; Tomasi, 1979).

The values of $A_{w\lambda}$ were obtained the same way as the $A_{g\lambda}$ previously, i.e. from MODTRAN results. In MODTRAN, both the selective band absorption and the continuum parameterizations have been considerably improved over those of LOWTRAN. The coefficients $A_{w\lambda}$ take both these two effects into consideration. It is important to note that MODTRAN absorption calculations are themselves based on HITRAN, a high resolution spectroscopic atlas for line-by-line calculations (Rothman et al., 1992). Although the relation between HITRAN and SMARTS2 is indirect and involves some smoothing and downgrading, it should retain enough accuracy for the applications envisioned here.

The band wing correction factor, B_w, is introduced to improve the parameterization away from the absorption band centers in varying humidity conditions. It has been obtained by analyzing several MODTRAN runs for different combinations of zenith angles and atmospheres.

It should be noted that because of the introduction of B_w and f_w in Eq. (12), the water vapor transmittance is not a simple function of the product $m_w w$, as it is in all simplified models (e.g. Leckner's), but rather a function of w, m_w, and p, as theory predicts (Gates and Harrop, 1963; Yamanouchi and Tanaka, 1985).

Precipitable water, w, needs to be carefully specified or accurately determined to obtain correct extinction calculations in the near infrared. For applications involving reference atmospheres, precalculated values are available, as explained in Section 2. Alternatively, for applications involving real atmospheric conditions, w can be indirectly measured by different experimental methods or estimated by using empirical relationships between w and the surface temperature and humidity (e.g. Garrison and Adler, 1990; Gueymard, 1994; Gueymard and Garrison, 1998; Leckner, 1978).
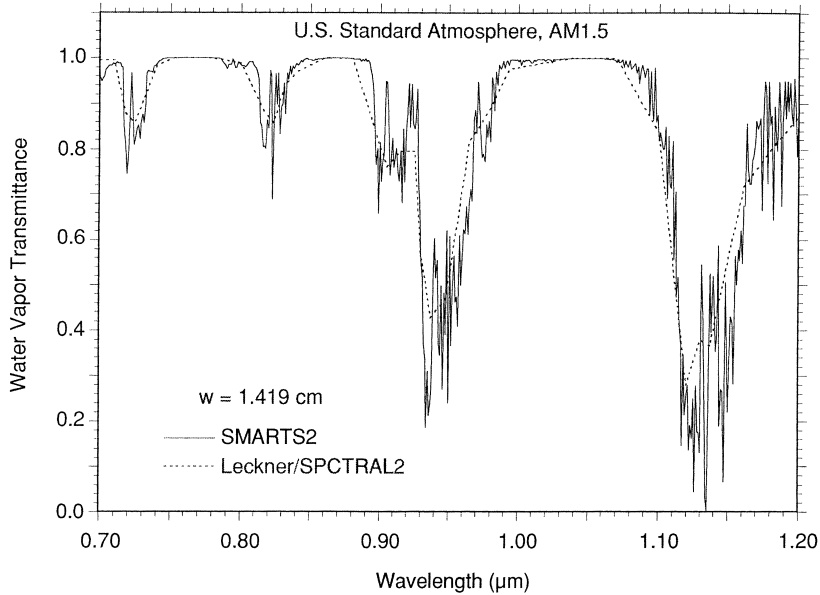
Fig. 4. Water vapor transmittance for the US Standard Atmosphere and an air mass of 1.5.

Figure 4 compares the water vapor transmittance in the 940 nm band as calculated by SMARTS2, and Leckner's model (as used in SPCTRAL2) for the US Standard Atmosphere ($w = 1.419$ cm) and an air mass of 1.5, thus corresponding to the ASTM and ISO standardized conditions (ASTM, 1987; ISO, 1992). The difference between the predictions of SMARTS2 and SPCTRAL2 is significant in some wavelength intervals, due to the latter's cruder resolution and older absorption data. Fig. 5 displays the same comparison, but with the Tropical Atmosphere ($w = 4.117$ cm) and a solar zenith angle of 80°

($m_w = 5.58$). Because of the increased total water vapor slant path (23 cm for Fig. 5, compared to 2.13 cm for Fig. 4), the spectral transmittance is extremely low between 930 and 960 nm. Also, the difference between the SPCTRAL2 and SMARTS2 transmittance predictions increases significantly.

3.6. Aerosol extinction

Spectral optical characteristics of both the tropospheric and stratospheric aerosols may change rapidly with time and with meteorological conditions. Although complete spectral determi-
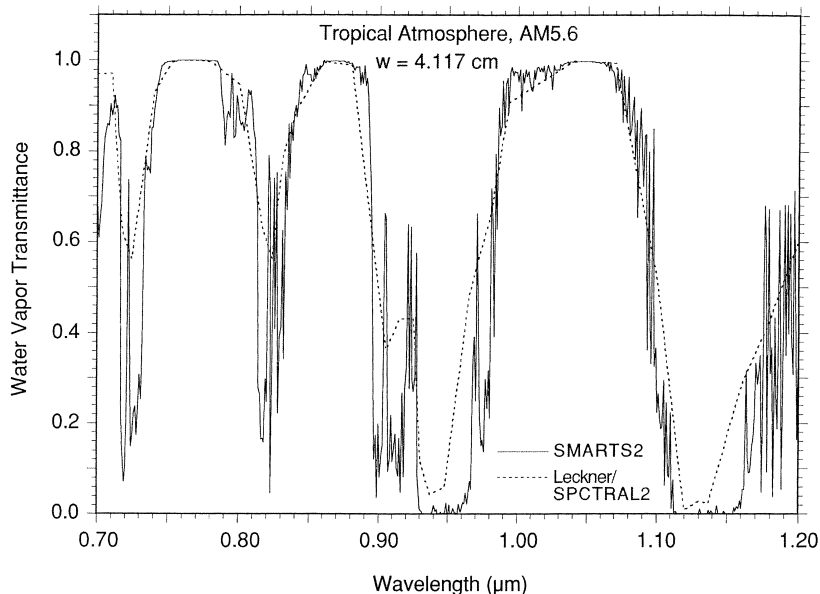
Fig. 5. Water vapor transmittance for a Tropical reference atmosphere and an air mass of 5.6.

nations of the aerosol optical thickness would actually be needed for detailed modeling, such measurements are rare, and in the best of cases, only broad climatological information is available, or indirect estimates of turbidity based on broadband irradiance or visibility data.

This general lack of detailed aerosol data justifies the use of a simplified methodology, namely the modified Ångström approach, which, as proposed by Bird (1984), considers only two different spectral regions, below and above $\lambda_0 = 0.5$ μm. The aerosol transmittance is obtained from the aerosol optical thickness, $\tau_{a\lambda}$, as:

$$T_{a\lambda} = \exp(-m_a \tau_{a\lambda}) \qquad (13)$$

with

$$\tau_{a\lambda} = \beta_i \, (\lambda/\lambda_1)^{-\alpha_i} \qquad (14)$$

where $\lambda_1 = 1$ μm, m_a is the aerosol optical mass from Eq. (A.1), $\alpha_i = \alpha_1$ if $\lambda < \lambda_0$ and α_2 otherwise, and finally $\beta_i = \beta_1 = 2^{\alpha_2 - \alpha_1}\beta$ if $\lambda < \lambda_0$ and $\beta_i = \beta_2 = \beta$ otherwise. Since $\tau_{a\lambda}$ is dimensionless in Eq. (14), it is explicitly written here as a function of a ratio, λ/λ_1, rather than a function of λ alone, as usually presented since Ångström. The dependence of the wavelength exponents α_1 and α_2 to the aerosol optical characteristics is discussed in Appendix B.

Although turbidity is expressed here with the Ångström coefficient, β (defined at 1 μm), it can also be defined in terms of two alternate coefficients: Schuëpp's B, or the optical thickness τ_{a5} (both defined at λ_0). The correspondence between β, B and τ_{a5} results from their respective definitions:

$$\tau_{a5} = 2^{\alpha_2}\beta \qquad (15)$$

$$B = \tau_{a5}/\ln 10. \qquad (16)$$

For an ideal Ångström aerosol ($\alpha_2 = 1.3$), Eq. (15) simplifies into $\beta = 0.406\tau_{a5}$. For an atmosphere laden with aerosols of larger size, α_2 would decrease to a typical value of 1.0, now producing $\beta = 0.5\tau_{a5}$. The latter relationship has been used, for example, to characterize the turbidity of the polluted atmosphere of Mexico City from spectral optical depth measurements at 500 nm and other wavelengths (Vasilyev et al., 1995).

Further correspondence between β, B, and the other frequently-used Linke and Unsworth–Monteith turbidity coefficients is physically derived elsewhere (Gueymard, 1998).

If turbidity data are not available, it is possible to estimate the aerosol optical thickness from ground observations of visibility. When observing a standard target under ideal conditions, as assumed by Koschmieder's theory (1924), the farthest distance at which such a target can be observed provides a theoretical definition of the *meteorological range*, V_r.

In practice, visibility (also called *visual range*, or more precisely, *prevailing visibility*) is reported at airports by human observers who use a few non-ideal markers irregularly spaced. Various difficulties complicate the observation conditions, so that visibility thus obtained is only a *crude estimate* of the desired meteorological range. (See the analyses for non-standard viewing conditions by Allard and Tombach (1981), Gordon (1979), Gorraiz et al. (1986) and Horvath (1971, 1981).) Visibility is also generally skewed towards low values (Reiss and Eversole, 1978). The WMO adopted a specific definition of visibility, called the meteorological optical range (MOR), which is different from Koschmieder's meteorological range, thus confusing the terminology. The formal relation between visibility or MOR, V, and meteorological range, V_r is $V_r = 1.306V$. But because of the fundamental disparity just explained between the 'practical' V and the 'theoretical' V_r, considerable spread can be expected in the exact correspondence between V_r and V when dealing with *actual* observations of V. Their average ratio has been observed to vary between 1.0 and 1.6, depending on local conditions (Gordon, 1979; Kneizys et al., 1980).

MODTRAN was run for different meteorological ranges, reference aerosols and surface humidities to obtain the corresponding value of τ_{a5}, from which β and B can be obtained from Eqs. (15) and (16). A fit of these results gives:

$$\beta = 0.55^{\alpha_2} \left[1.3307 \, (V_r^{-1} - V_m^{-1})^{0.614} \right.$$
$$\left. + 3.4875(V_r^{-1} - V_m^{-1}) \right] \qquad (17)$$

where $V_m = 340.85$ km is the theoretical maximum meteorological range, obtained for a pure Rayleigh atmosphere corresponding to $\beta = 0$. No additional dependence on the particular reference aerosol or its relative humidity could be isolated. Eq. (17) is proposed here as a replacement for the King and Buckius equation (1979), which was based on a now outdated aerosol model — and later incorrectly attributed to Selby and McClatchey in Iqbal's textbook (1983). The predictions of the two equations are compared in Fig. 6 which shows that Eq. (17) predicts significantly larger turbidities for meteorological ranges below about 50 km.
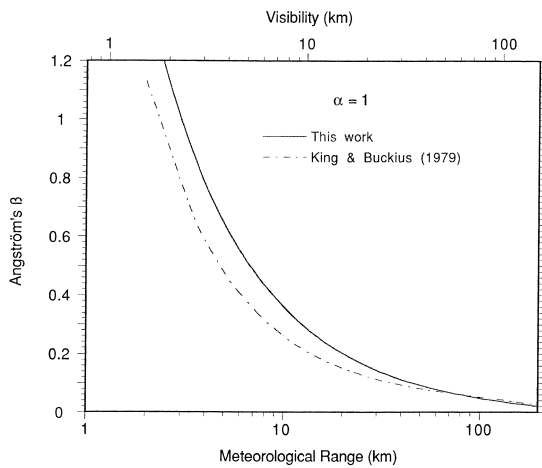
Fig. 6. Turbidity vs. visibility and meteorological range.

For the reasons noted above, it is emphasized that Eq. (17) can provide an acceptable estimate of β only at those sites where visibility data are of consistent quality. In many cases, the environment around the observer's site cannot provide the necessary fixed markers beyond a certain distance. The turbidity estimates with Eq. (17) are then incorrectly skewed toward large values and an anomalously feeble inverse correlation is observed between V and β (El-Wakil *et al.*, 2001).

Figure 7 presents a comparison of the transmittances for the S&F (Shettle and Fenn, 1979) rural aerosol and the USSA atmospheric conditions, as predicted by SMARTS2, MODTRAN, and SPCTRAL2. The latter simply uses Eq. (14) with $\alpha_1 = \alpha_2 = 1.14$ (i.e. the straight Ångström model). Both SMARTS2 and SPCTRAL2 have been used with $\tau_{a5} = 0.3442$, a value that generates the same

aerosol transmittance at 500 nm than a meteorological range of 25 km in MODTRAN. It should be noted that the ASTM/ISO standard for direct irradiance (ASTM, 1987; ISO, 1992) is based on $\tau_{a5} = 0.27$, a value said to correspond to $V_r = 25$ km according to both Bird *et al.* (1983) and to versions 4 or earlier of LOWTRAN — or incorrectly, to 23 km according to ASTM (1987) and ISO (1992). This correspondence between $V_r = 25$ km and $\tau_{a5} = 0.27$ results from the same outdated aerosol model used by King and Buckius and therefore does not appear appropriate anymore. MODTRAN uses a more recent and detailed aerosol model (Shettle, 1989; Shettle and Fenn, 1979) which explicitly considers the direct effect of humidity on the optical properties of aerosols; this is the same detailed reference aerosol model that has been used here to obtain Table B.1 and Eq. (B.1). However, as partially illustrated in Fig. 7, MODTRAN evaluates the aerosol transmittance at only 13 wavelengths between 280 and 4000 nm, and linearly interpolates between these. Due to the actual curvature of the continuous transmittance function, this oversimplification in MODTRAN underestimates the aerosol transmittance if $\alpha > 0$ (the case of Fig. 7), or overestimates it otherwise, between the calculated reference points.

4. CIRCUMSOLAR RADIATION

The direct beam radiation calculated so far comes ideally from the solar disk only. When comparing such *calculations* to measured data, it is important to take into account the circumsolar
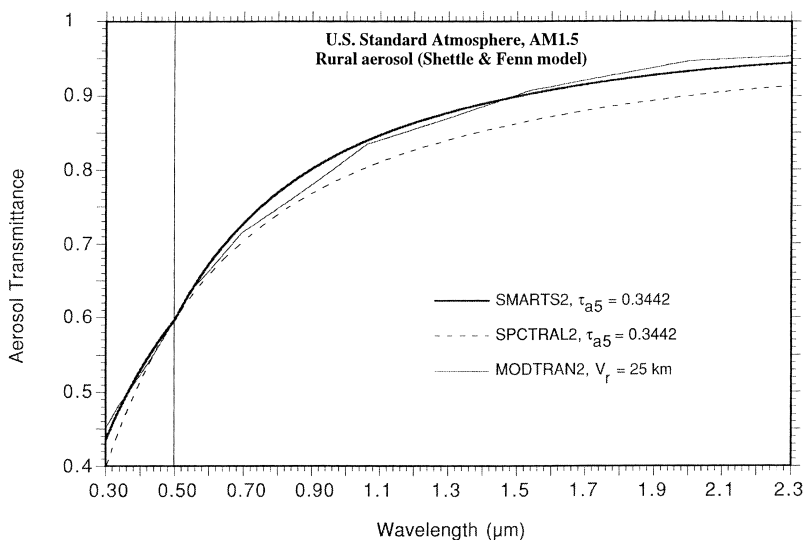

Fig. 7. Aerosol transmittance predicted by SMARTS2 and other models for a meteorological range of 25 km.

diffuse radiation that is also intercepted in the aperture (typically a 1–10° full angle) of the actual radiometer. This circumsolar contribution is a function of the size distribution in the aerosol column and increases with turbidity and optical mass. The circumsolar radiance within the solar aureole decreases sharply with the angular distance from the sun's center (i.e. the scattering angle). Because the circumsolar irradiance from the sky is non-negligible compared to the sun's direct beam irradiance, at least in certain conditions (Fröhlich and Quenzel, 1974; Grassl, 1971; Shah, 1978), a correction factor needs to be applied to the calculated spectral beam irradiance if a radiometer with a field of view larger than the solar disk is to be simulated.

The radiometer optical geometry is important for precise calculations (Ångström, 1961). The 'aperture' angle mentioned above is the full angle determined by the exterior aperture of the instrument as viewed from the *central point* of the receiver. The *opening angle*, ξ_o is defined as half this aperture angle. It is the most commonly reported characteristic of a radiometer's optical geometry. The *slope angle*, ξ_s, and *limit angle*, ξ_l, are the minimum and maximum half viewing angles, respectively, at which any beam will strike the receiver area directly, with $\xi_s < \xi_o < \xi_l$. This means that for an incidence angle, ξ, below ξ_s, the receiver will be fully efficient (100% response), whereas for $\xi > \xi_l$ the receiver will ideally detect no signal (0% response). For intermediate incidence angles, the response will be partial, as described by the geometric *penumbra function*, $P(\xi)$, derived by Pastiels (1959) and used by others (e.g. Major, 1994).

The calculation of the circumsolar correction factor is rather involved because the atmospheric scattering properties vary widely with both the aerosol optical characteristics and wavelength. The maximum circumsolar effect is known to occur around 0.4–0.5 μm, with negligible contributions in the infrared beyond 1.5 μm. A circumsolar correction factor, $F_{c\lambda}$, to be multiplied by the pure direct beam irradiance, is used here to approximate the latter's experimental counterpart:

$$F_{c\lambda} = 1 + E_{dc\lambda}/E_{bn\lambda} \tag{18}$$

where $E_{bn\lambda}$ is defined in Eq. (3), and the circumsolar irradiance, $E_{dc\lambda}$, results from the spatial integration of the spectral sky radiance within the total field of view of the radiometer. As the circumsolar radiance varies strongly with the scattering angle but only slightly with azimuth,

the azimuthally averaged radiance that exists along the *almucantar*, $L_{a\lambda}(\xi)$, is conventionally used to avoid a double angle integration over the aureole (Box and Deepak, 1979, 1981). The circumsolar irradiance detected by the radiometer is then (see e.g. Major, 1994; Putsay, 1980, 1995a)

$$E_{dc\lambda} = 2\pi \int_0^{\xi_l} L_{a\lambda}(\xi)P(\xi)\sin\xi\cos\xi\,d\xi. \tag{19}$$

Because multiple scattering from aerosol particles is only marginal in the aureole, at least for scattering angles below 10° (Box and Deepak, 1978), it will be neglected here, thus simplifying calculations. The conventional single-scattering approximation to the almucantar radiance (Volz, 1987) can thus be used, with the addition of two correction terms which explicitly include multiple scattering by *molecules* and backscattering after multiple reflections from the ground (Box and Deepak, 1979, 1981). The almucantar radiance is finally expressed as:

$$L_{a\lambda}(\xi) = m_a E_{bn\lambda}\left[(\tau_{R\lambda} + \tau_{mR\lambda})\,F_R(\xi) \right.$$
$$\left. + \tau_{mg\lambda}F_R(0°) + \varpi_0\tau_{a\lambda}\,F_{a\lambda}(\xi)\right] \tag{20}$$

where m_a is calculated in Eq. (A.1), $\tau_{R\lambda}$ in Eq. (5), and $\tau_{a\lambda}$ in Eq. (14). $F_R(\xi)$ is the phase function for Rayleigh scattering (normalized here to 1), which, according to Lenoble (1993), may be obtained from

$$F_R(\xi) = [3/(4 + 2\delta)][1 + \delta + (1 - \delta)\cos^2\xi]/4\pi \tag{21}$$

where δ is the depolarization factor that appeared in Eq. (4). $F_{a\lambda}(\xi)$ is the aerosol phase function, also normalized to 1, which describes the forward-peaked scattering pattern of the aerosol particles. This function is specific to each aerosol's size distribution and refractive index and is normally calculated from Mie theory. To simplify calculations in SMARTS2, a library of call-up functions of ξ, obtained by fitting published discrete data of $F_{a\lambda}(\xi)$ for $\xi \leq 10°$, is used. The spectral phase functions for the different Shettle and Fenn aerosol models have been fitted from the tabulated data in MODTRAN. The phase function for Braslau and Dave's aerosol models C and C1 (based on Deirmendjian's *Haze L*) has been fitted from data in Lenoble (1985). Finally, the spectral phase functions for the three SRA aerosols have also been fitted from discrete calculations obtained by Putsay (1995a,b). Examples of such

phase functions are shown in Figs. 8 and 9 for rural and maritime aerosol models, respectively.

The only terms that remain to be evaluated in Eq. (20) are ϖ_0, $\tau_{mR\lambda}$, and $\tau_{mg\lambda}$. The first term is the aerosol single-scattering albedo, which is discussed in Appendix B. The second term corresponds to a fictitious optical thickness due to molecular multiple scattering. A fit of the data tabulated by Box and Deepak (1979) gives:

$$\tau_{mR\lambda} = 1.38(\tau_{R\lambda} + \varpi_0\tau_{a\lambda})^2. \tag{22}$$

The third term corresponds to augmentation of the radiance by backscattering processes between the ground and the atmosphere. It is simply obtained as (Box and Deepak, 1979):

$$\tau_{mg\lambda} = \rho_{g\lambda}(\tau_{R\lambda} + \tau_{mR\lambda}) \tag{23}$$

where $\rho_{g\lambda}$ is the spectral ground albedo.

The integral in Eq. (19) cannot be evaluated analytically, so it is approximated numerically using angular intervals of 0.1° and Simpson's rule. The circumsolar correction factors obtained with this method for different wavelengths and air masses compare well to some test cases (Putsay, 1995b; Tomasi *et al.*, 1989).
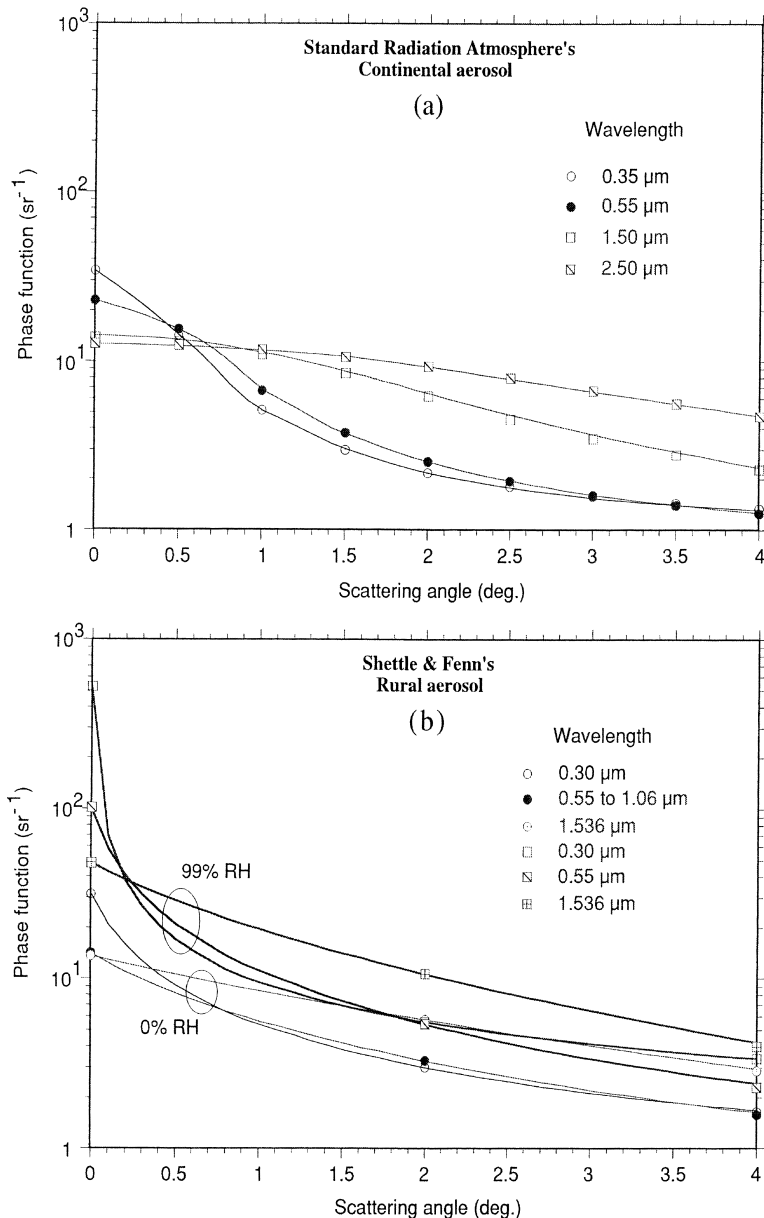

Fig. 8. Phase functions for different aerosol models. (a) SRA continental aerosol; (b) Shettle and Fenn's rural aerosol. Symbols indicate original data and continuous lines their least squares fits.
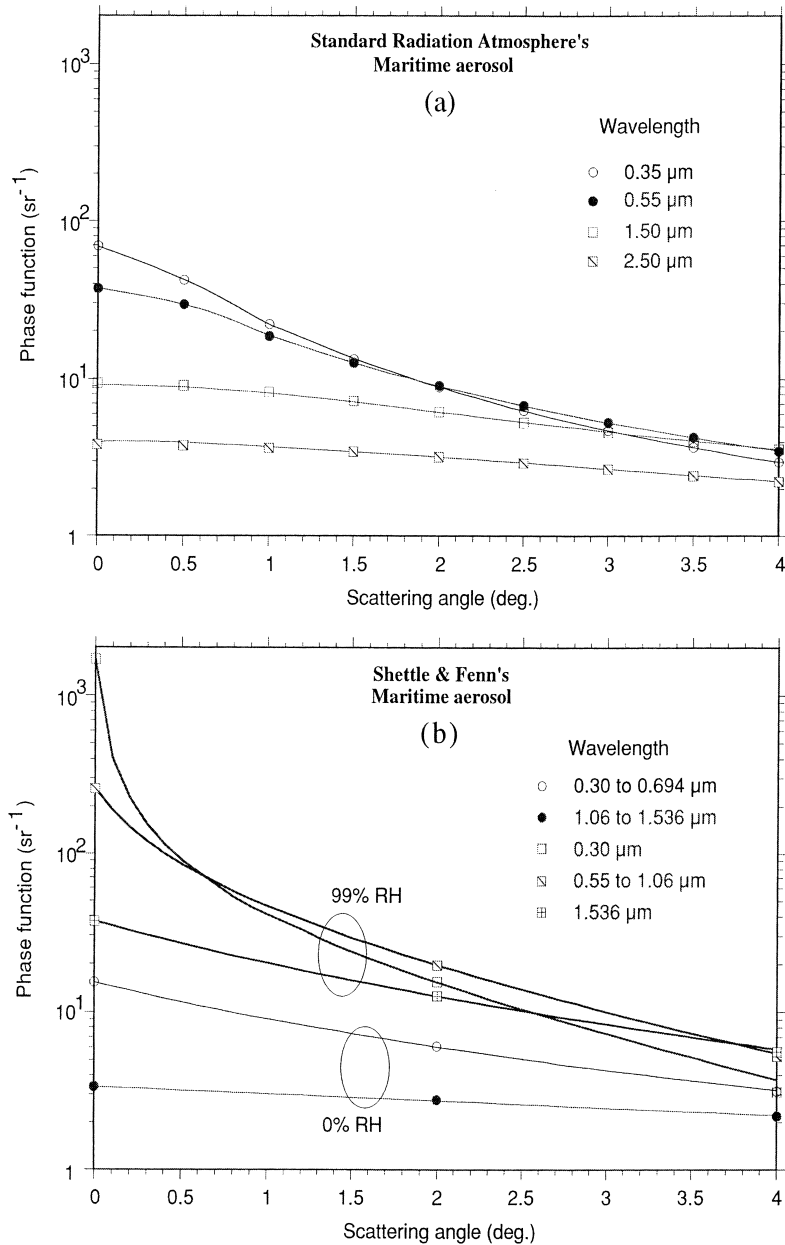
Fig. 9. Phase functions for different maritime aerosols.

As demonstrated by Fig. 10, the ratio of circumsolar radiation to beam radiation is highly variable, depending on solar zenith angle, wavelength, humidity, and aerosol optical characteristics. Obviously, the circumsolar contribution also increases with the radiometer's aperture angle. The increased circumsolar contribution from maritime aerosols compared to rural aerosols may be attributed to their steeper forward-peaking phase function (compare Figs. 8 and 9).

When analyzing the *broadband* irradiance measured with different radiometers, or when predicting the effective irradiance on solar concentrators, a circumsolar correction is needed to obtain the true direct irradiance from the 'apparent' irradiance (direct + circumsolar), or vice versa. This correction is obtained by integrating Eq. (18) over the full spectrum. Using these numerical results, a simple parameterization for this important correction has been proposed for different apertures and aerosol models (Gueymard, 1998). Other broadband calculations involving different aerosol models have been carried out elsewhere (e.g. Thomalla *et al.*, 1983). All these results are in good agreement about the magnitude of the circumsolar correction and its dependence on the
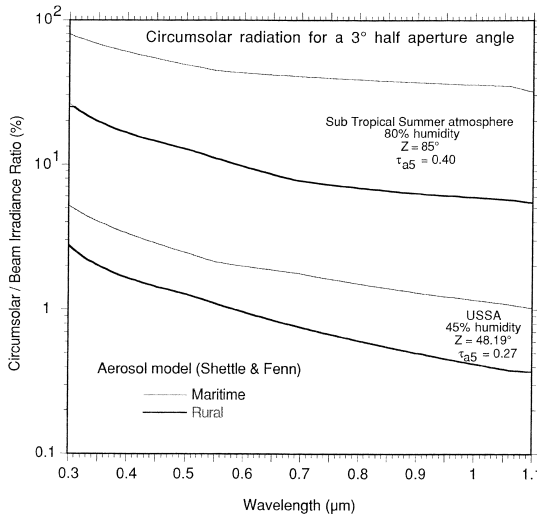
Fig. 10. Spectral circumsolar contribution for different atmospheric conditions.

receiver's geometry, the aerosol optical characteristics, and the sun's zenith angle.

5. OUTPUT DATA SMOOTHING

Spectroradiometric instruments are characterized by having different spectral bandpass shapes and widths. The Gaussian and triangular shapes are chosen here as representative (Fig. 11). A useful feature of SMARTS2 is a post-processor that scans the raw outputs (transmittances or irradiances) and smooths them to derive new outputs at optional relaxed bandwidths, approximating instrumental transmittance characteristic
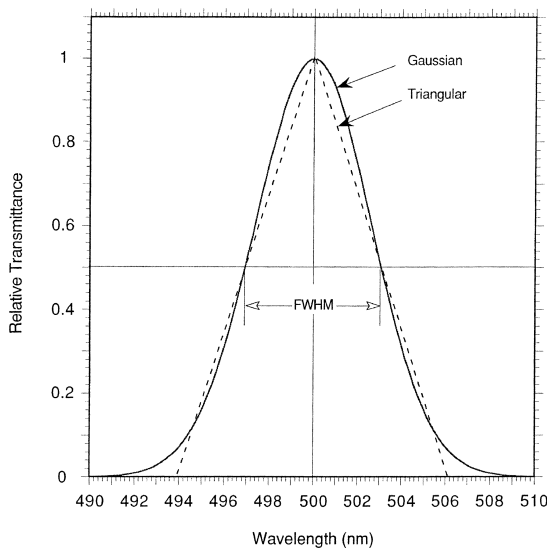

Fig. 11. Examples of smoothing functions for the simulation of spectroradiometers.

by a Gaussian or triangular function with a given bandwidth, characterized by its *full width at half maximum* (FWHM). This is similar to the optional postprocessor in MODTRAN, except that the latter is limited to a triangular function. It is essential to perform such a data smoothing prior to comparing modeled and measured data. In the case of Gaussian filtering for example, the weight applied to the irradiance or transmittance at wavelength λ is obtained with an equation form identical to that of a normal distribution with a mean λ_c and standard deviation σ, except for the normalizing coefficient (1 instead of $[2\pi]^{-0.5}$):

$$W(\lambda) = \exp\left[-\frac{(\lambda - \lambda_c)^2}{2\sigma^2} \right] \qquad (24)$$

where λ_c is the wavelength corresponding to the peak transmittance, and $\sigma = \text{FWHM} (8 \ln 2)^{-0.5}$ is such that $W(\lambda) = 0.5$ if $\lambda = \lambda_c + \text{FWHM}/2$. It is stressed that this exercise of simulating a radiometer supposes that it is ideal; in particular, its transmittance is assumed perfectly symmetric around λ_c. For a non ideal instrument, Eq. (24) would have to be replaced by a more specific function.

The broadened, or smoothed, value of a spectral variable $X(\lambda)$, irradiance or transmittance, is finally obtained numerically as:

$$\overline{X} = \sum_{\lambda_n}^{\lambda_x} W(\lambda)X(\lambda) / \sum_{\lambda_n}^{\lambda_x} W(\lambda) \qquad (25)$$

where $\lambda_n = \lambda_c - \Delta\lambda$ and $\lambda_x = \lambda_c + \Delta\lambda$, $\Delta\lambda$ being the greatest integer smaller than (or equal to) $\text{FWHM}/d\lambda + 3$, where $d\lambda$ is the wavelength interval of the original spectrum (1 nm below 1700 nm and 5 nm above, with the present extraterrestrial spectrum). For example, for $\lambda_c = 500$ nm, $\text{FWHM} = 6$ nm, $d\lambda = 1$ nm, the numerical integration in Eq. (25) would be carried out between $\lambda_n = 491$ and $\lambda_x = 509$ nm. For this example, the excluded transmitted irradiance would be only 0.2% on either side of the integration limits. For slightly expanded integration limits (to 490–510 nm), this result would become a negligible 0.045%.

6. PERFORMANCE ASSESSMENT

As SMARTS2 is intended to be used in a variety of applications, its accuracy is a critical factor and needs to be assessed under different atmospheric conditions. Incidentally, it must be pointed out that a numerical model cannot be 'validated' or 'verified' — despite the frequent

usage of these terms in this field — because of fundamental reasons critically reviewed by Oreskes *et al.* (1994). This is why the term 'performance assessment' is used exclusively here.

To obtain spectral irradiances — rather than just transmittances — from Eq. (3), $E_{0n\lambda}$ must be defined at the same wavelengths used in all calculations. In the UV, between 280 and 412 nm, recent satellite data were obtained from Michael van Hoosier (personal communication, 1994). They consist of the low-resolution version of measurements made on March 19, 1992 during a period of quiet sun with the SUSIM (Solar Ultraviolet Spectral Irradiance Monitor) instrument on board the Upper Atmosphere Research Satellite (UARS), as described by Brueckner *et al.* (1993). Data points listed at 0.25-nm intervals were reduced to a 1-nm step with a trapezoidal rule. For the visible and near-IR range (412–4000 nm) the data used here reflect the revised extraterrestrial spectrum introduced in version 3 of MODTRAN: its high-resolution spectrum has been degraded, with only a few minor corrections. The 280–4000 nm integrated extraterrestrial spectrum used here totals 1349.7 W/m^2, compared to 1349.5 W/m^2 for the WMO-standard spectrum, as tabulated by Wehrli (1985). These irradiances are consistent with the WMO-standard value of 1367 W/m^2 for the whole spectrum, i.e. the so-called 'solar constant'.

A comparison between SMARTS2 and the B&D model (Dave *et al.*, 1975) can be made for a 60° zenith angle, an MLS atmosphere, and B&D's aerosol model *Haze L*, case C1. The beam normal irradiances are compared in Fig. 12, and show generally good agreement, although some differences are apparent in limited spectral ranges. (All the rigorous codes discussed in this section used older tabulations of $E_{0n\lambda}$. Their results have been corrected to match SMARTS2's $E_{0n\lambda}$, so that the remaining variance between the respective terrestrial spectra is only due to differences in modeling the atmospheric processes.) In the near IR, these differences are most probably caused by the less detailed or accurate water vapor and mixed gases absorption data that were available in the early 1970s when the B&D model was devised. In the visible, the differences in predicted irradiances between about 500 and 700 nm may be caused by differences in handling the aerosol optical characteristics. As mentioned earlier in Section 3.6, the aerosol optical thickness of the B&D aerosol model shows significant departure from the Ångström equation. This translates into a slight but spectrally-broad discrepancy between the transmittance predictions.

The predictions of SMARTS2 and BRITE (a Monte-Carlo code described by Bird and Hulstrom, 1982) were also analyzed. Their predicted direct normal irradiances are compared in Fig. 13, based on the tabulations of Bird *et al.* (1983), Hulstrom *et al.* (1985), and ASTM (1987). The conditions are: US Standard Atmosphere, $\tau_{a5} = 0.27$
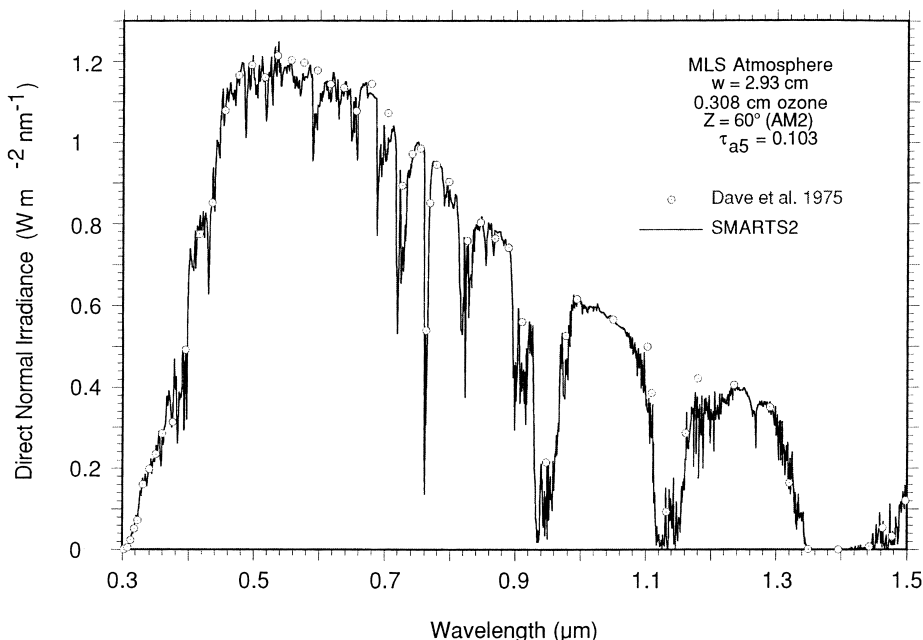

Fig. 12. Direct normal irradiance predicted by SMARTS2 and Dave *et al.* (1975) for an MLS atmosphere.
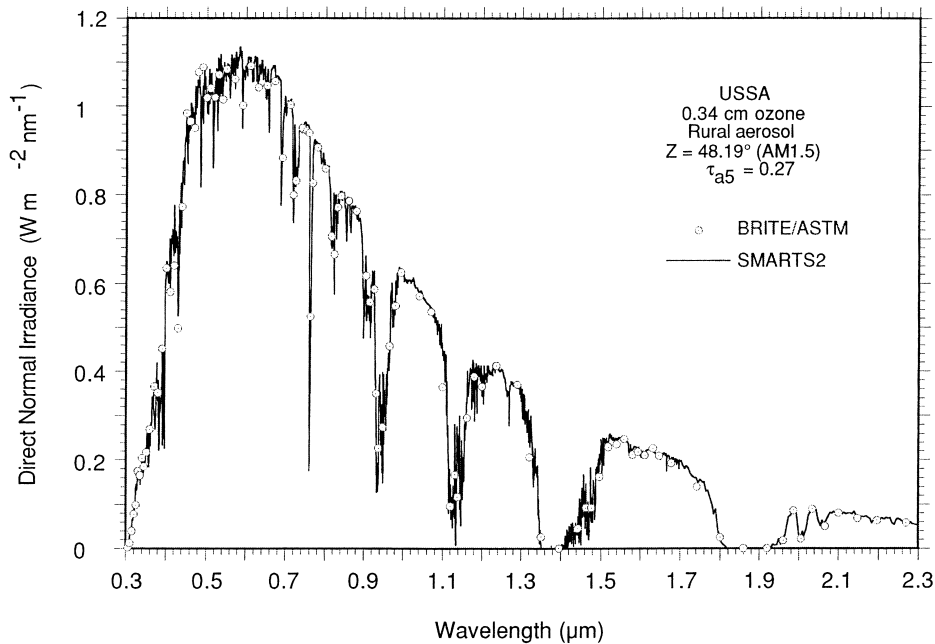
Fig. 13. Beam normal irradiance predicted by SMARTS2 and BRITE for the US Standard Atmosphere.

using the SRA continental aerosol model in SMARTS2 to approximate the preliminary version of S&F rural model internal to BRITE, a constant ground reflectance of 0.2, circumsolar radiation admitted within a 3° opening angle, and $Z=48.19°$ (air mass 1.5). The ASTM/ISO standard spectra (ASTM, 1987; ISO, 1992) are for direct beam irradiance at normal incidence, as shown in Fig. 13. It is clear from Fig. 13 that the predictions of SMARTS2 and BRITE are in close agreement, which suggests that SMARTS2 can be used to interpolate within the irradiance standards (using more practical *constant* intervals), to extrapolate these standards to wavelengths below their current lower limit of 305 nm, or to generate spectra for other 'typical' conditions. (BRITE, the basic code behind these standards, is no longer available; therefore, no new run can be performed.)

Because the tabulations of Hulstrom *et al.* (1985) and the ASTM/ISO standards are for an 'experimental' direct normal irradiance (with circumsolar radiation), whereas those of Bird *et al.* (1983) are for ideal irradiance without the circumsolar contribution, it is possible to obtain the circumsolar contribution alone in this particular case by simple subtraction, wavelength by wavelength. This provides a way of assessing the performance of the circumsolar algorithm described in Section 4. SMARTS2 was run both with the SRA continental aerosol and the S&F rural aerosol, which produced similar results.

BRITE's results were originally obtained for a preliminary rural model of Shettle and Fenn which did *not* consider humidity effects. As shown in Fig. 14, the agreement between the SMARTS2 and BRITE predictions is close, even though the aerosol models used in the two codes are not exactly identical. In this particular case, the circumsolar effect adds about 2.5% to the beam irradiance at 300 nm, decreasing to 1.2% at 500 nm, and to about 0.5% at 1100 nm. The apparent discontinuities in BRITE's results may be caused by its stochastic nature.

Detailed comparison against carefully measured data is the classic way to assess the performance of a model. This exercise also shows that SMARTS2's accuracy is within the experimental uncertainty. A preliminary assessment suggested good agreement between its predictions and experimental spectroradiometric data obtained in Spain (Utrillas *et al.*, 1998). Further detailed assessment results will be reported subsequently.

7. CONCLUSION

The spectral model presented here closely fits the most recently available extinction data. It can be used to generate terrestrial spectra needed in various sensitivity analyses, to rapidly approximate the predictions of more rigorous codes (e.g. MODTRAN), or to simulate spectroradiometric results from atmospheric data. Its capabilities extend well into the UV region (down to 280 nm),
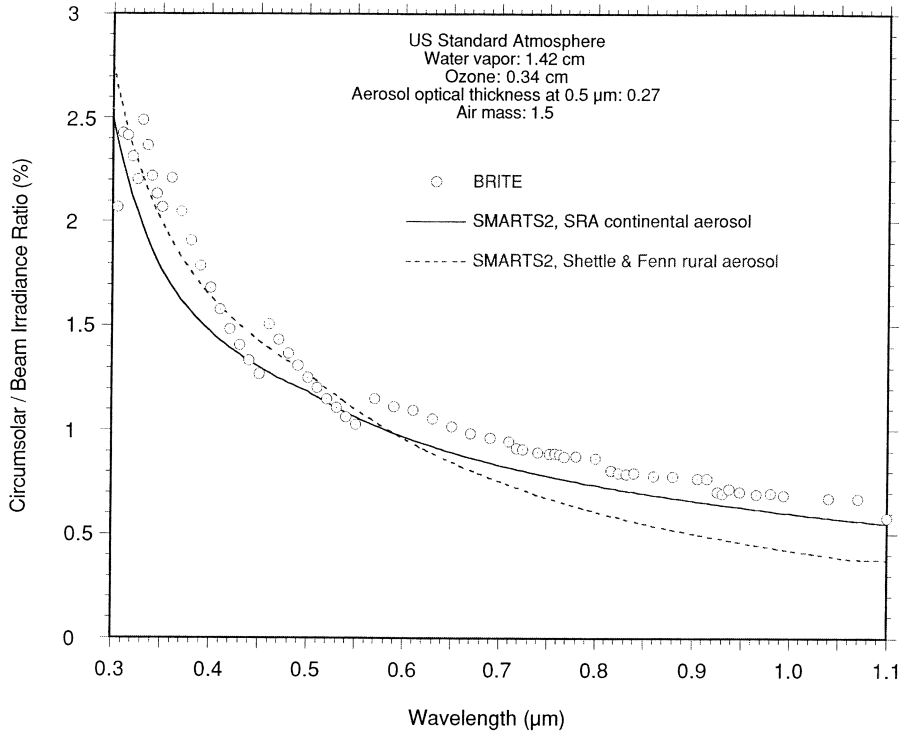
Fig. 14. Relative contribution of circumsolar radiation as predicted by SMARTS2 and BRITE for the conditions of the ASTM/ISO standard.

where it uses a recently measured extraterrestrial spectrum, and into the near-IR (up to 4000 nm). Specific comparisons show discernible differences between the individual transmittances evaluated here and those obtained with older models, such as those of Leckner (1978) and Bird and Riordan (1986).

A limited performance assessment, using comparisons with other predictions from rigorous codes in a variety of atmospheric conditions, shows that SMARTS2's direct irradiance performs well and consistently.

Another application of SMARTS2 resides in its capability to generate reference spectra close to the existing standard ASTM/ISO terrestrial spectra, but with higher resolution and flexibility.

Future publications will be devoted to a more detailed performance assessment of this model, using reference measured data in particular.

The Fortran code of SMARTS2 and related information (including an expanded version of this report) is available online (http://homepage.mac.com/smarts2).

NOMENCLATURE

a	exponent in Eq. (11)
$a_1 - a_4$	coefficients of Eq. (5)
$A_{g\lambda}$	mixed gas absorption coefficient (cm^{-1})
$A_{n\lambda}$	nitrogen dioxide absorption coefficient (cm^{-1})
$A_{o\lambda}$	ozone absorption coefficient (cm^{-1})
$A_{w\lambda}$	water vapor absorption coefficient (cm^{-1})
B	Schüepp turbidity coefficient
B_w	correction factor for band wing absorption
c	wavelength-dependent exponent in Eq. (12)
$c_0 - c_2$	coefficients of Eq. (2)
C_t	correction factor for the abundance of O_3 and NO_2
$E_{bn\lambda}$	spectral beam irradiance $(W/m^2\ nm)$
$E_{dc\lambda}$	parasitic circumsolar diffuse radiation $(W/m^2\ nm)$
$E_{on\lambda}$	extraterrestrial irradiance $(W/m^2\ nm)$
$f_0 - f_5$	coefficient for Eq. (10)
$F_{a\lambda}(\xi)$	aerosol phase function
$F_{c\lambda}$	circumsolar correction factor for a radiometer
$F_R(\xi)$	phase function for Rayleigh scattering
f_w	pressure scaling factor
FWHM	full width half maximum (nm)
H_R	atmospheric scale height (8.4345 km at 15°C)
$L_{a\lambda}(\xi)$	sky radiance along the almucantar $(W/m^2\ nm\ sr)$
m	exponent in Eq. (1)
m_a	aerosol optical mass
m_g	mixed gas optical mass
m_n	nitrogen dioxide optical mass
m_o	ozone optical mass
m_R	optical air mass
m_w	water vapor optical mass
n	exponent in Eq. (1); exponent in Eq. (12)
n_0	refractive index of air
N_0	number of density of molecules (2.547305×10^{25} m^{-3} at 288.15 K)
p	site's pressure (mb)
P	pressure ratio, p/p_0
$P(\xi)$	penumbra function of a radiometer
p_0	sea-level pressure (1013.25 mb)
T	air temperature (K)
$T_{a\lambda}$	spectral aerosol transmittance

T_{en}	effective NO_2 temperature (K)
T_{eo}	effective ozone temperature (K)
$T_{g\lambda}$	spectral mixed gas transmittance
$T_{n\lambda}$	spectral nitrogen dioxide transmittance
T_o	spectral ozone transmittance
T_{rn}	reference laboratory temperature for NO_2 absorption (243.2 K)
T_{ro}	reference laboratory temperature for ozone absorption (228 K)
$T_{R\lambda}$	spectral Rayleigh transmittance
$T_{w\lambda}$	spectral water vapor transmittance
u_g	scale height for mixed gases (km)
u_n	nitrogen dioxide abundance (atm-cm)
u_o	ozone abundance (atm-cm)
V	visability (km)
V_m	maximum meteorological range (340.85 km)
V_r	meteorological range (km)
w	precipitable water (cm)
$W(\lambda)$	spectral weighting coefficient
z	elevation (km)
Z	sun's zenith angle (rad)

Greek symbols

α	Ångström wavelength exponent for the whole spectrum
α_1	Ångström wavelength exponent for $\lambda < \lambda_0$
α_2	Ångström wavelength exponent for $\lambda > \lambda_0$
β	Ångström turbidity coefficient
β_1	Ångström turbidity coefficient for $\lambda < \lambda_0$
β_2	Ångström turbidity coefficient for $\lambda > \lambda_0$
δ	depolarization factor
θ	temperature ratio, $288.15/T$
λ	wavelength (nm)
λ_0	limiting wavelength (500 nm)
λ_1	reference wavelength for β (1000 nm)
λ_C	central wavelength (nm)
ξ	scattering angle (rad)
ξ_1	limit angle of a radiometer (rad)
ξ_o	opening angle of a radiometer (rad)
ξ_s	slope angle of a radiometer (rad)
ρ_a	air density (kg/m^3)
$\rho_{g\lambda}$	spectral ground albedo
ρ_v	water vapor density (kg/m^3)
τ_{a5}	aerosol optical thickness at 500 nm
$\tau_{a\lambda}$	aerosol optical thickness
$\tau_{mg\lambda}$	optical thickness due to backscattering
$\tau_{mR\lambda}$	optical thickness due to molecular multiple scattering
$\tau_{o\lambda}$	ozone optical thickness
$\tau_{R\lambda}$	Rayleigh optical thickness
ϖ_0	aerosol single-scattering albedo

APPENDIX A. SUN POSITION AND OPTICAL MASSES

The sun's apparent position is defined by its zenith angle and its azimuth. These angles are in turn obtained as a function of declination and hour angle through the algorithm described in the *Astronomical Almanac* (Nautical Almanac Office, 1992). It has been shown by Michalsky (1988) to have an excellent accuracy, better than 0.01° for declination.

Most simplified models use a single optical mass (usually the optical mass for air molecules or 'air mass') to estimate the total slant path for all the extinction processes in the atmosphere. Different optical masses are considered here because each extinction process corresponds to a particular vertical concentration profile. Consideration of separate optical masses improves the model accuracy at large zenith angles, as they differ substantially above about 80°. The optical mass formulae have been fitted to the data rigorously calculated by Miskolczi *et al.* (1990). Other rigorous data at large zenith angles, from recent determinations including Mie scattering (Sarkissian, 1995; Sarkissian *et al.*, 1995), were also added to better fit the optical masses of O_3 and NO_2. The selected fitting function is similar to that proposed by Kasten (1965) and Kasten and Young (1989) but with better overall accuracy, and the physical advantage of predicting a correct air mass of exactly 1.0 for a zenith sun:

$$m_i = [\cos Z + a_{i1} Z^{a_{i2}} (a_{i3} - Z)^{a_{i4}}]^{-1} \qquad (A.1)$$

where m_i stands for m_R (Rayleigh), m_a (aerosols), m_n (NO_2), m_o (O_3), m_g (mixed gases) or m_w (water vapor), Z is the zenith angle, and the coefficients a_{ij} appear in Table A.1. The values of m_i for $Z = 90°$ are also indicated in Table A.1, showing a wide dispersion between 16.6 (for O_3) and 71.4 (for water vapor and aerosols). In particular, the *air mass* thus calculated for $Z = 90°$ is 38.1304, in good agreement with other rigorously determined values, such as 38.1665 (Miskolczi *et al.*, 1990) and 38.0868 (Kasten and Young, 1989).

Because of the model's capability to handle large zenith angles and optical masses, and the way the latter were defined in the first place (Young, 1974), it is stressed that the optical masses need to be used in conjunction with the *apparent* solar zenith angle, i.e. the true (astronomical) zenith angle minus refraction. Refraction is calculated according to the *Astronomical Almanac*, as a function of zenith angle, pressure, and temperature. Situations for which the sun's disk is visible while its zenith angle is larger than 90° are rare but possible, e.g. at sunrise/sunset in mountainous areas with an open horizon, or as

Table A.1. Coefficients for the optical masses, Eq. (A.1)

Extinction process	a_{i1}	a_{i2}	a_{i3}	a_{i4}	m_i @ $Z = 90°$
Rayleigh	4.5665E−1	0.07	96.4836	−1.6970	38.130
Ozone	2.6845E+2	0.5	115.420	−3.2922	16.601
Nitrogen dioxide[a]	6.0230E+2	0.5	117.960	−3.4536	17.331
Mixed gases	4.5665E−1	0.07	96.4836	−1.6970	38.130
Water vapor	3.1141E−2	0.1	92.4710	−1.3814	71.443
Aerosols	3.1141E−2	0.1	92.4710	−1.3814	71.443

[a] For *stratospheric* NO_2 only; use the water vapor mass for *tropospheric* NO_2 and a weighted average for a combination of the two.

viewed from an airplane. To avoid numerical instability with Eq. (A.1), the apparent zenith angle is limited to 91°, corresponding to a true astronomical angle of about 92°.

APPENDIX B. AEROSOL RADIATIVE PROPERTIES

Representative values of the wavelength exponents α_1 and α_2 have been obtained by linearly fitting (in log–log coordinates) the spectral optical coefficients of different reference aerosol models to Eq. (14). This process is illustrated in Fig. B.1 for a rural aerosol and shows that it is well described by the Angström model ($\alpha = 1.3$), except in the UV. The four reference aerosols defined by Shettle and Fenn (1979), hereafter S&F, were used in LOWTRAN (starting with version 5) and MODTRAN, and their optical characteristics were tabulated for relative humidities between 0 and 99% in this cited report. The corresponding values of α_1 and α_2 obtained with the fitting technique explained above are

given in Table B.1. As it clearly shows, α_1 is always less than α_2, the average ratio α_1/α_2 is close to 0.7 for rural, urban, and maritime aerosols at relative humidities $\leq 70\%$, and finally both α_1 and α_2 tend to decrease when relative humidity increases. This shows that the original Angström model (i.e. with $\alpha_1 = \alpha_2$ in Eq. (14)) is not appropriate for these reference aerosol models.

A fit of the data in Table B.1 gives α_1 and α_2 from relative humidity, RH, and aerosol type:

$$\alpha_1 = (C_1 + C_2 X_{rh})/(1 + C_3 X_{rh}) \quad \text{(B.1a)}$$

$$\alpha_2 = (D_1 + D_2 X_{rh} + D_3 X_{rh}^2)/(1 + D_4 X_{rh}) \quad \text{(B.1b)}$$

where coefficients C_i and D_i are found in Table B.2 and $X_{rh} = \cos (0.9RH)$ with an argument in degrees.

In the Braslau and Dave (hereafter B&D) atmospheric model (Braslau and Dave, 1973), no effect of relative humidity on the properties of the aerosol (of the *Haze L* type) is considered, which
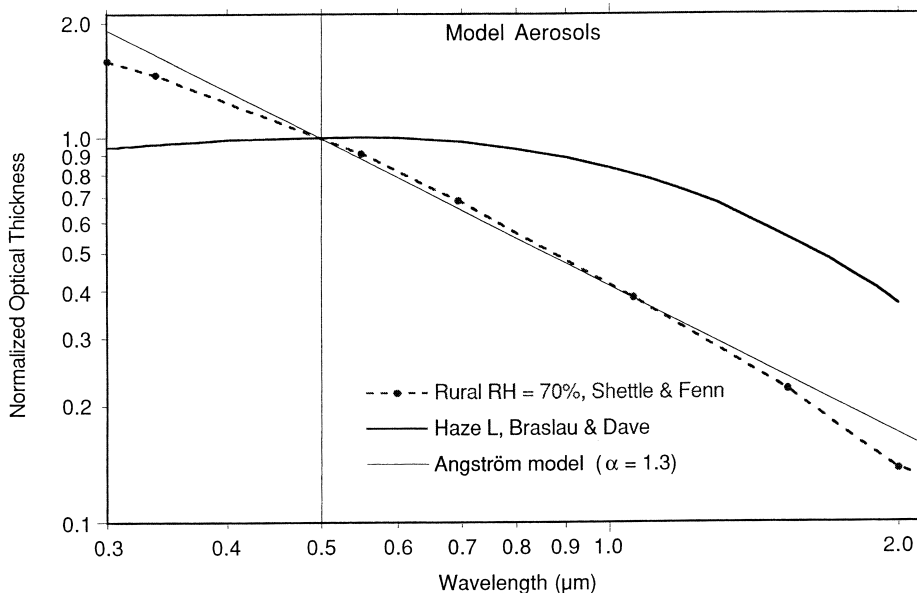

Fig. B.1. Aerosol optical thickness (normalized to 0.5 μm) as a function of wavelength for selected aerosol models.

Table B.1. Wavelength exponents for different aerosol models (Shettle and Fenn, 1979)

Relative humidity		0%	50%	70%	80%	90%	95%	98%	99%
Rural	α_1	0.933	0.932	0.928	0.902	0.844	0.804	0.721	0.659
	α_2	1.444	1.441	1.428	1.376	1.377	1.371	1.205	1.134
Urban	α_1	0.822	0.827	0.838	0.829	0.779	0.705	0.583	0.492
	α_2	1.167	1.171	1.186	1.229	1.256	1.252	1.197	1.127
Maritime	α_1	0.468	0.449	0.378	0.226	0.232	0.195	0.141	0.107
	α_2	0.626	0.598	0.508	0.286	0.246	0.175	0.098	0.053
Tropospheric	α_1	1.010	1.008	1.005	0.980	0.911	0.864	0.797	0.736
	α_2	2.389	2.379	2.357	2.262	2.130	2.058	1.962	1.881

simplifies calculations. However, the aerosol optical thickness departs significantly from the Angström model, i.e. α actually varies considerably more with wavelength than this simple model predicts, as Fig. B.1 illustrates. A significant gain of accuracy in the modeling of this relatively rare spectral behavior is obtained with the two-band split described by Eq. (14). Using the same fitting technique as before, the resulting values of α_1 and α_2 are -0.311 and 0.265, respectively. The negative sign of α_1 indicates that $\tau_{a\lambda}$ actually *decreases* with wavelength below about 500 nm, contrary to the 'normal' behavior. A negative α_1

and a positive α_2 result in a flattened bell-shaped curve when plotting $\tau_{a\lambda}$ as a function of λ (Fig. B.1). Such a case may in fact be characteristic of maritime polar air masses, as observed in different circumstances by Weller and Leiterer (1988).

A more recent and frequently used aerosol model is the preliminary standard known as the SRA (Standard Radiation Atmosphere) from IAMAP (1986). The relative humidity is here simply assumed to be 'below 70%', and thus without a direct effect on the optical characteristics of any of the three different aerosol types considered: continental, industrial and maritime.

Table B.2. Coefficients of Eq. (B.1) for different aerosol models (Shettle and Fenn, 1979)

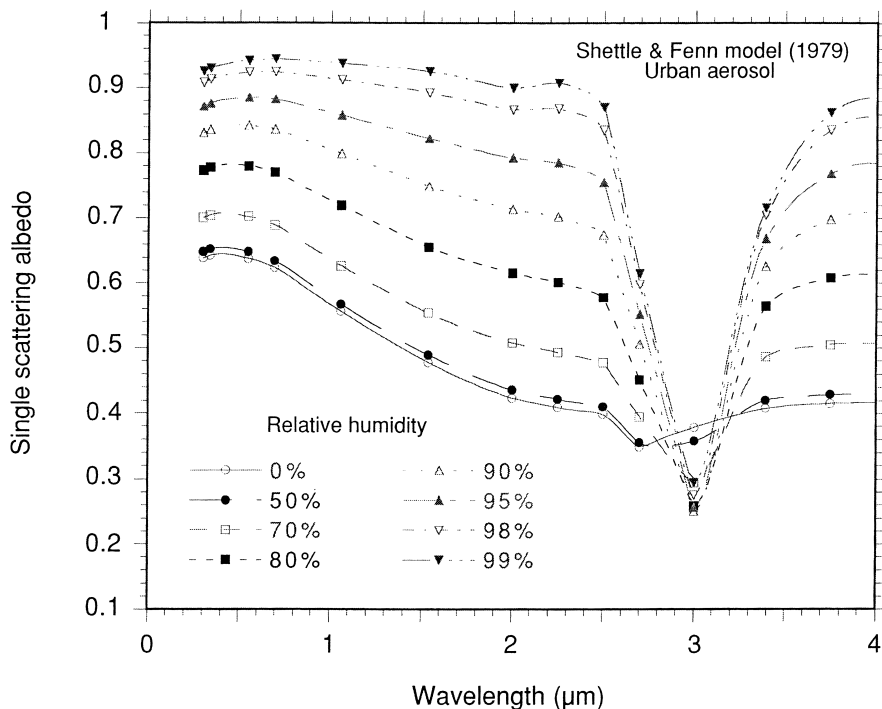| Coefficient	C_1	C_2	C_3	D_1	D_2	D_3	D_4
Rural	0.581	16.823	17.539	0.8547	78.696	0	54.416
Urban	0.2595	33.843	39.524	1.0	84.254	-9.1	65.458
Maritime	0.1134	0.8941	1.0796	0.04435	1.6048	0	1.5298
Tropospheric	0.6786	13.899	13.313	1.8379	14.912	0	5.96

Fig. B.2. Spectral single-scattering albedo of urban aerosol as affected by relative humidity.

The average values of α_1, again obtained by linearly fitting the extinction coefficients, are respectively 0.940, 1.047 and 0.283, and those of α_2 are 1.335, 1.472 and 0.265. Data for other reference aerosols may be found elsewhere (d'Almeida *et al.*, 1991), but some of the numerous tables this reference contains may be incorrect (personal communication with Eric P. Shettle, 1994).

The single-scattering albedo, ϖ_0, is a fundamental optical characteristic of aerosols, equal to 1.0 for a perfectly non-absorbing aerosol. For a real aerosol, it normally varies with relative humidity and wavelength. The B&D and SRA reference aerosols do not consider any humidity effect. To the contrary, ϖ_0 is strongly dependent on both wavelength and humidity for the different reference aerosols of the S&F model (Shettle and Fenn, 1979). This is illustrated in Fig. B.2 for the case of the urban aerosol. Because of the complex dependence on humidity and wavelength, the value of ϖ_0 is difficult to parameterize, but suitable functions of λ and RH have been found for each aerosol model.

REFERENCES

Allard D. and Tombach I. (1981) The effects of non-standard conditions on visibility measurements. *Atmos. Environ.* **15**, 1847–1857.

Anderson G. P., Chetwynd J. H., Theriault J. M., Acharya P., Berk A., Robertson D. C., Kneizys F. X., Hoke M. L., Abreu L. W. and Shettle E. P. (1993) MODTRAN2: suitability for remote sensing. In Proceedings of the Conference on Atmospheric Propagation and Remote Sensing II, Vol. 1968, Kohnle A. and Miller W. B. (Eds.), pp. 514–525, SPIE, Orlando.

Anderson G. P., Clough S. A., Kneizys F. X., Chetwynd J. H. and Shettle E. P. (1986) AFGL atmospheric constituent profiles (0–120 km). In *Technical report AFGL-TR-86-0110*, Air Force Geophysics Laboratory, Hanscom AFB, MA.

Anderson S. M. (1992) Laser measurements of ozone absorption cross sections in the Chappuis band. *Geophys. Res. Lett.* **19**, 933–936.

Anderson S. M. (1993) Ozone absorption cross section measurements in the Wulf bands. *Geophys. Res. Lett.* **20**, 1579–1582.

Ångström A. (1961) Radiation to actinometric receivers in its dependence on aperture conditions. *Tellus* **13**, 425–431.

Anon (1966). *US Standard Atmosphere supplements, 1966*, ESSA/NASA/USAF, US Government Printing Office, Washington, DC.

Asano S. and Uchiyama A. (1987) Application of an extended ESFT method to calculation of solar heating rates by water vapor absorption. *J. Quant. Spectrosc. Radiat.* **38**, 147–158.

ASTM (1987). *Standard Tables for Terrestrial Direct Normal Solar Spectral Irradiance for Air Mass 1.5, Standard No. E891-87*, American Society for Testing and Materials, Philadelphia, PA.

Berk A., Bernstein L. S. and Robertson D. C. (1989). *MODTRAN: A Moderate Resolution Model for LOWTRAN7, Report GL-TR-89-0122*, Air Force Geophysical Laboratory, Hanscom, MA.

Bird R. E. (1984) A simple, solar spectral model for direct-
normal and diffuse horizontal irradiance. *Solar Energy* **32**, 461–471.

Bird R. E. and Hulstrom R. L. (1982) Extensive modeled solar spectral data sets with solar cell analysis. In *Technical report SERI/TR-215-1598*, Solar Energy Research Institute, Golden, CO.

Bird R. E., Hulstrom R. L. and Lewis L. J. (1983) Terrestrial solar spectral data sets. *Solar Energy* **30**, 563–573.

Bird R. E. and Riordan C. (1986) Simple solar spectral model for direct and diffuse irradiance on horizontal and tilted planes at the Earth's surface for cloudless atmospheres. *J. Clim. Appl. Meteorol.* **25**, 87–97.

Box M. A. and Deepak A. (1978) Single and multiple scattering contributions to circumsolar radiation. *Appl. Opt.* **17**, 3794–3797.

Box M. A. and Deepak A. (1979) Atmospheric scattering corrections to solar radiometry. *Appl. Opt.* **18**, 1941–1949.

Box M. A. and Deepak A. (1981) An approximation to multiple scattering in the earth's atmosphere: almucantar radiance formulation. *J. Atmos. Sci.* **38**, 1037–1048.

Braslau N. and Dave J. V. (1973) Effect of aerosols on the transfer of solar energy through realistic model atmospheres. *J. Appl. Meteorol.* **30**, 601–619.

Brine D. T. and Iqbal M. (1983) Diffuse and global solar spectral irradiance under cloudless skies. *Solar Energy* **30**, 447–453.

Brueckner G. E., Edlow K. L., Floyd L. E., Lean J. L. and VanHoosier M. E. (1993) The Solar Ultraviolet Spectral Irradiance Monitor (SUSIM) experiment on board the Upper Atmosphere Research Satellite (UARS). *J. Geophys. Res.* **98D**, 10695–10711.

Cacciani M., di Sarra A., Fiocco G. and Amoruso A. (1989) Absolute determination of the cross sections of ozone in the wavelength region 339–355 nm at temperatures 220–293 K. *J. Geophys. Res.* **94D**, 8485–8490.

Coffey M. T. (1988) On the temporal change of stratospheric NO_2. *Geophys. Res. Lett.* **15**, 331–334.

Coffey M. T., Mankin W. G. and Goldman A. (1981) Simultaneous spectroscopic determination of the latitudinal, seasonal and diurnal variability of stratospheric N_2O, NO, NO_2 and HNO_3. *J. Geophys. Res.* **86C**, 7331–7341.

d'Almeida G. A., Koepke P. and Shettle E. P. (1991). *Atmospheric Aerosols: Global Climatology and Radiative Characteristics*, A. Deepak, Hampton, VA.

Daumont D., Brion J., Charbonnier J. and Malicet J. (1992) Ozone UV spectroscopy I: absorption cross-sections at room temperature. *J. Atmos. Chem.* **15**, 145–155.

Dave J. V., Halpern P. and Braslau N. (1975) Spectral distribution of the direct and diffuse solar energy received at sea-level of a model atmosphere. In *Technical report G320-3332*, IBM Palo Alto Scientific Center.

Davidson J. A., Cantrell C. A., McDaniel A. H., Shetter R. E., Madronich S. and Calvert J. G. (1988) Visible–ultraviolet absorption cross sections for NO_2 as a function of temperature. *J. Geophys. Res.* **93D**, 7105–7112.

Elansky N. F., Arabov A. Y., Elokhov A. S. and Senik I. A. (1984) Spatial and temporal variability of the NO_2 total content based on annual observation data. In *Atmospheric Ozone (Proceedings of the Quadriennal Ozone Symposium)*, Zerefos C. S. and Ghazi A. (Eds.), pp. 157–162, D. Reidel, Halkidiki, Greece.

El-Wakil S. A., El-Metwally M. and Gueymard C. (2001) Atmospheric turbidity of urban and desert areas of the Nile Basin in the aftermath of Mt. Pinatubo's eruption. *Theor. Appl. Clim.* **68**, 89–108.

Fröhlich C. and Quenzel H. (1974) Influence of the sun's aureole on the determination of turbidity. In *Observation and Measurement of Atmospheric Pollution*, Special Environmental Report No. 3, WMO No. 368, World Meteorological Organization, Geneva.

Garrison J. and Adler G. P. (1990) Estimation of precipitable water over the United States for application to the division of solar radiation into its direct and diffuse components. *Solar Energy* **44**, 225–241.

Gates D. M. and Harrop W. J. (1963) Infrared transmission of the atmosphere to solar radiation. *Appl. Opt.* **2**, 887–898.

Gordon J. I. (1979) Daytime visibility, a conceptual review. In *Report AFGL-TR-79-0257*, Visibility Laboratory, UCSD, San Diego, CA.

Gorraiz J., Horvath H. and Raimann G. (1986) Influence of small color differences on the contrast threshold: its application to atmospheric visibility. *Appl. Opt.* **25**, 2537–2545.

Grassl H. (1971) Calculated circumsolar radiation as a function of aerosol type, field of view, wavelength and optical depth. *Appl. Opt.* **10**, 2542–2543.

Gueymard C. (1993a) Development and performance assessment of a clear sky spectral radiation model. In *Proceedings 22nd ASES Conference, Solar '93*, pp. 433–438, American Solar Energy Society, Washington, DC.

Gueymard C. (1993b) Mathematically integrable parameterization of clear-sky beam and global irradiances and its use in daily irradiation applications. *Solar Energy* **50**, 385–397.

Gueymard C. (1994) Analysis of monthly average atmospheric precipitable water and turbidity in Canada and Northern United States. *Solar Energy* **53**, 57–71.

Gueymard C. (1998) Turbidity determination from broadband irradiance measurements: a detailed multi-coefficient approach. *J. Appl. Meteorol.* **37**, 414–435.

Gueymard C. and Garrison J. D. (1998) Critical evaluation of precipitable water and atmospheric turbidity in Canada using measured hourly solar irradiance. *Solar Energy* **62**, 291–307.

Horvath H. (1971) On the applicability of the Koschmieder visibility formula. *Atmos. Environ.* **5**, 177–184.

Horvath H. (1981) Atmospheric visibility. *Atmos. Environ.* **15**, 1785–1796.

Hulstrom R., Bird R. and Riordan C. (1985) Spectral solar irradiance data sets for selected terrestrial conditions. *Solar Cells* **15**, 365–391.

Husar R. B. and White W. H. (1976) On the color of the Los Angeles smog. *Atmos. Environ.* **10**, 199–204.

IAMAP (1986) A preliminary cloudless standard atmosphere for radiation computation. In *Report WCP-112, WMO/TD-No. 24*, World Meteorological Organization, Geneva, Switzerland.

Iqbal M. (1983). *An Introduction To Solar Radiation*, Academic Press, Toronto.

ISO (1992). *Solar energy — Reference solar spectral irradiance at the ground at different receiving conditions, pt. 1, International Standard 9845-1*, International Organization for Standardization, Geneva.

Justus C. G. and Paris M. V. (1985) A model for solar spectral irradiance and radiance at the bottom and top of a cloudless atmosphere. *J. Clim. Appl. Meteorol.* **24**, 193–205.

Kambezidis H. D., Adamopoulos A. D. and Gueymard C. (2001) Total NO_2 column amount over Athens, Greece in 1996–97. *Atmos. Res.* **57**, 1–8.

Kasten F. (1965) A new table and approximation formula for the relative optical air mass. *Arch. Met. Geoph. Biokl.* **B14**, 206–223.

Kasten F. and Young A. T. (1989) Revised optical air mass tables and approximation formula. *Appl. Opt.* **28**, 4735–4738.

Keating G. M., Pitts M. C. and Young D. F. (1990) Ozone reference models for the middle atmosphere. *Adv. Space Res.* **10**, 317–355.

Kerker M. (1969). *The Scattering of Light and other Electromagnetic Radiation*, Academic Press, New York.

King R. and Buckius R. O. (1979) Direct solar transmittance for a clear sky. *Solar Energy* **22**, 297–301.

Kneizys F. X., Shettle E. P., Gallery W. O., Chetwynd Jr. J. H., Abreu L. W., Selby J. E. A., Fenn R. W. and McClatchey R. A. (1980) Atmospheric transmittance/radiance: computer code LOWTRAN 5. In *Report AFGL TR-80-0067*, Air Force Geophysics Laboratory, Hanscom AFB, MA.

Koepke P. and Quenzel H. (1978) Water vapor: spectral transmission at wavelengths between 0.7 μm and 1 μm. *Appl. Opt.* **17**, 2114–2118.

Koschmieder H. (1924) Theorie der horizontalen Sichtweite. *Beitr. Phys. Atmos.* **12**, 33–53.

Leckner B. (1978) The spectral distribution of solar radiation at the Earth's surface — elements of a model. *Solar Energy* **20**, 143–150.

Lenoble J. (1985). *Radiative Transfer in Scattering and Absorbing Atmospheres: Standard Computational Procedures*, A. Deepak, Hampton, VA.

Lenoble J. (1993). *Atmospheric Radiative Transfer*, A. Deepak, Hampton, VA.

Liley J. B., Johnston P. V., McKenzie R. L., Thomas A. J. and Boyd I. S. (2000) Stratospheric NO_2 variations from a long series at Lauder, New Zealand. *J. Geophys. Res.* **105D**, 11633–11640.

London J. (1977) Distribution of atmospheric ozone and how it is measured. In *Air Quality Meteorology and Atmospheric Ozone*, ASTM Special Publication 653, Wheeler J. B. et al. (Ed.), American Society for Testing and Materials, Philadelphia, PA.

Major G. (1994) Circumsolar correction for pyrheliometers and diffusometers. In *Report WMO/TD-No. 635*, World Meteorological Organization, Geneva.

Matthews L. K., Mulholland G. P. and Stevens M. (1987) Measurement and analysis of solar spectral irradiance. *Proceedings ASME/JSME/JSES Solar Engineering Conference*, Honolulu, HI, pp. 307–313.

McCartney E. J. (1976). *Optics in the Atmosphere*, Wiley, New York.

McKenzie R. L. and Johnston P. V. (1984) Southern hemisphere nitrogen dioxide. In *Atmospheric Ozone, Proceedings Quadriennal Ozone Symposium*, Zerefos C. S. and Ghazi A. (Eds.), pp. 163–167, D. Reidel, Halkidiki, Greece.

Michalsky J. J. (1988) The Astronomical Almanac's algorithm for approximate solar position (1950–2050). *Solar Energy* **40**, 227–235, Erratum, Solar Energy, 41 (1988) 113.

Miskolczi F. M. et al. (1990) High resolution atmospheric radiance-transmittance code (HARTCODE). In *Meteorology and Environmental Sciences*, p. 770, World Scientific, Singapore.

Molina L. T. and Molina M. J. (1986) Absolute absorption cross sections of ozone in the 185- to 350-nm wavelength range. *J. Geophys. Res.* **91D**, 14501–14508.

Mount G. H., Rusch D. W., Noxon J. F., Zawodny J. M. and Barth C. A. (1984) Measurements of stratospheric NO_2 from the solar mesosphere explorer satellite — 1. An overview of the results. *J. Geophys. Res.* **89D**, 1327–1340.

Narrow-band Spectral Radiation Data Acquisition, Analysis and Modeling, Report No. IEA-SHCP-17C-1, Nann S. and Bakenfelder A. (Eds.), (1993). Zentrum für Sonnenenergie- und Wasserstoff-Forschung, Stuttgart, Germany.

Nann S. and Riordan C. (1991) Solar spectral irradiance under clear and cloudy skies: measurements and a semiempirical model. *J. Appl. Meteorol.* **30**, 447–462.

Nautical Almanac Office (1992). *The Astronomical Almanac*, Nautical Almanac Office, Washington.

Noxon J. F. (1978) Tropospheric NO_2. *J. Geophys. Res.* **83C**, 3051–3057.

Noxon J. F. (1979) Stratospheric NO_2 — 2. Global behavior. *J. Geophys. Res.* **84C**, 5067–5076, Correction, J. Geophys. Res., 85C (1980) 4560–4561.

Oreskes N., Shrader-Frechette K. and Belitz K. (1994) Verification, validation and confirmation of numerical models in the Earth sciences. *Science* **263**, 641–646.

Pastiels R. (1959). *Contribution à l'étude du problème des méthodes actinométriques, Publ. A11*, Institut Royal Météorologique de Belgique, Uccle, Belgium.

Peck E. R. and Reeder K. (1972) Dispersion of air. *J. Opt. Soc. Am.* **62**, 958–962.

Pierluissi J. H., Maragoudakis C. E. and Tehrani-Movahed R. (1989) New LOWTRAN band model for water vapor. *Appl. Opt.* **28**, 3792–3795.

Pierluissi J. H. and Tomiyama K. (1980) Numerical methods for the generation of empirical and analytical transmittance functions with applications to atmospheric trace gases. *Appl. Opt.* **19**, 2298–2309.

Pierluissi J. H. and Tsai C. M. (1986) Molecular transmittance band model for oxygen in the visible. *Appl. Opt.* **25**, 2458–2460.

Pierluissi J. H. and Tsai C. M. (1987) New LOWTRAN models for the uniformly mixed gases. *Appl. Opt.* **26**, 616–618.

Putsay M. (1980) The effect of circumsolar radiation on accuracy of turbidity measurements. *Időjárás* **84**, 261–267.

Putsay M. (1995a) Circumsolar radiation calculated for various aerosol models. *Időjárás* **99**, 67–76.

Putsay M. (1995b) *Spectral tabulations of aerosol phase functions, atmospheric radiance and circumsolar irradiance*, Personal communication.

Reiss N. M. and Eversole R. A. (1978) Rectification of prevailing visibility statistics. *Atmos. Environ.* **12**, 945–950.

Ridgway W. L. and Arking A. (1986) Parameterization of near infrared absorption by atmospheric gases. In *Preprint 6th Conference Atmospheric Radiation, Williamsburg, VA*, pp. 190–193, American Meteorological Society.

Riordan C. (1990). *SPCTRAL2, Fortran computer program printout*, Personal communication.

Rothman L. S. et al. (1992) The HITRAN molecular database: editions of 1991 and 1992. *J. Quant. Spectrosc. Radiat.* **48**, 469–507.

Sarkissian A. (1995). *Values of air-mass factors predicted with eight radiative transfer models*, Personal communication.

Sarkissian A., Roscoe H. K., Fish D., Van Roozendael M., Gil M., Chen H. B., Wang P., Pommereau J. P. and Lenoble J. (1995) Ozone and NO_2 air-mass factors for zenith-sky spectrometers: intercomparison of calculations with different radiative transfer models. *Geophys. Res. Lett.* **22**, 1113–1116.

Schneider W., Moortgat G. K., Tyndall G. S. and Burrows J. P. (1987) Absorption cross-sections of NO_2 in the UV and visible region (200–700 nm) at 298 K. *J. Photochem. Photobiol.* **40**, 195–217.

Schroeder R. and Davies J. A. (1987) Significance of nitrogen dioxide in estimating aerosol optical depth and size distributions. *Atmos. Ocean* **25**, 107–114.

Shah G. M. (1978) Aperture effects on atmospheric turbidity measurements. *Solar Energy* **21**, 527–530.

Shettle E. P. (1989) Models of aerosols, clouds and precipitation for atmospheric propagation studies. In Proceedings of the Conference on Atmospheric Propagation in the UV, Visible, IR and mm-Wave Region and Related Systems Aspects, Copenhagen, Denmark, Vol. 454, p. 15.1, AGARD.

Shettle E. P. and Fenn R. W. (1979) Models for the aerosols of the lower atmosphere and the effects of humidity variations on their optical properties. In *Report AFGL-TR-79-0214*, Air Force Geophysics Laboratory, Hanscom, MA.

Smith R. C., Wan Z. and Baker K. S. (1992) Ozone depletion in Antarctica: modeling its effect on solar UV irradiance under clear-sky conditions. *J. Geophys. Res.* **97C**, 7383–7397.

Song G., Xiuji Z. and Xisochun Z. (1994) O_3, SO_2, NO_2 and UVB measurements in Beijing and baseline station of northwestern part of China. In Proceedings of the Conference on Ozone in the Troposphere and Stratosphere, Vol. 2, Hudson R. D. (Ed.), pp. 746–748, NASA, Charlottesville, VA, Conference publication 3266.

Teillet P. M. (1990) Rayleigh optical depth comparisons from various sources. *Appl. Opt.* **29**, 1897–1900.

Thomalla E., Köpke P., Müller H. and Quenzel H. (1983) Circumsolar radiation calculated for various atmospheric conditions. *Solar Energy* **30**, 575–587.

Tomasi C. (1979) Non-selective absorption by atmospheric water vapour at visible and near infrared wavelengths. *Q. J. R. Meteorol. Soc.* **105**, 1027–1040.

Tomasi C. et al. (1989) Antarctic sky diffuse radiance in sun-photometric measurements. In *Proceedings of the Conference on Italian Research on Antarctic Atmosphere*, pp. 105–119, SIF, Bologna.

Utrillas M. P., Bosca J. V., Martinez-Lozano J. A., Cañada J., Tena F. and Pinazo J. M. (1998) A comparative study of SPCTRAL2 and SMARTS2 parameterized models based on spectral irradiance measurements at Valencia (Spain). *Solar Energy* **63**, 161–171.

Vasilyev O. B., Contreras A. L., Velazquez A. M., Fabi R. P., Ivlev L. S., Kovalenko A. P., Vasilyev A. V., Jukov V. M. and Welch R. M. (1995) Spectral optical properties of the polluted atmosphere of Mexico City (spring–summer 1992). *J. Geophys. Res.* **100D**, 26027–26044.

Vigroux E. (1953) Contribution à l'étude expérimentale de l'absorption de l'ozone. *Ann. Phys.* **8**, 709–762.

Volz F. E. (1987) Measurements of the skylight scattering function. *Appl. Opt.* **26**, 4098–4105.

Wehrli C. (1985). *Extraterrestrial Solar Spectrum*, World Radiation Center, Davos, Switzerland, Publication no. 615.

Weller M. and Leiterer U. (1988) Experimental data on spectral aerosol optical thickness and its global distribution. *Beitr. Phys. Atmos.* **61**, 1–9.

Yamanouchi T. and Tanaka M. (1985) Absorption properties of the near-infrared water vapor bands. *J. Quant. Spectrosc. Radiat.* **34**, 463–472.

Young A. T. (1974) Observational technique and data reduction. In Astrophysics, pt. A: Optical and Infrared, Vol. 12, Carleton N. (Ed.), Academic Press, New York.

Young A. T. (1981) On the Rayleigh-scattering optical depth of the atmosphere. *J. Appl. Meteorol.* **20**, 328–330.